Report No. KS-21-01 ▪ FINAL REPORT ▪ January 2021

Predicting Critical Shear Stress of Fine-Grained Soils in Kansas

Stacey Kulesza, Ph.D., P.E.
Md Zahidul Karim, Ph.D.

Kansas State University Transportation Center

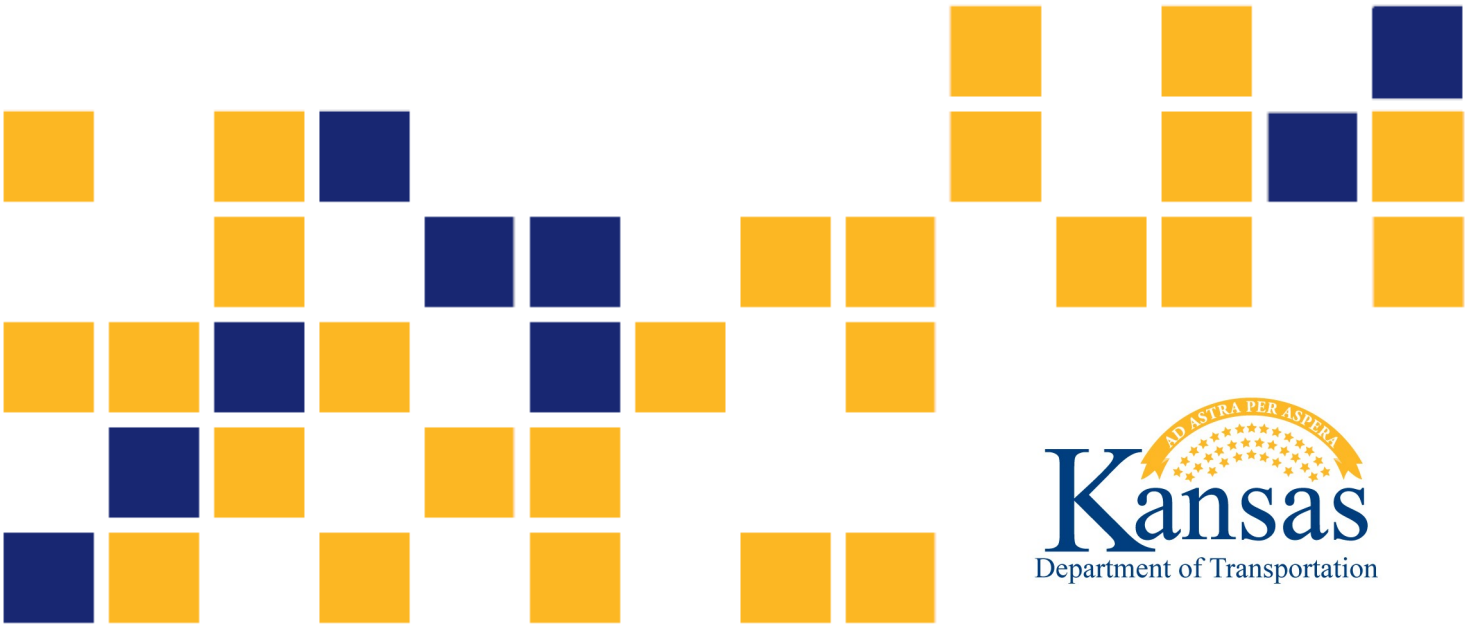

Kansas
Department of Transportation

1 Report No. KS-21-01	**2 Government Accession No.**	**3 Recipient Catalog No.**
4 Title and Subtitle Predicting Critical Shear Stress of Fine-Grained Soils in Kansas		**5 Report Date** January 2021 **6 Performing Organization Code**
7 Author(s) Stacey Kulesza, Ph.D., P.E. Md Zahidul Karim, Ph.D.		**8 Performing Organization Report No.**
9 Performing Organization Name and Address Kansas State University Transportation Center Department of Civil Engineering 2118 Fiedler Hall Manhattan, KS 66506-5000		**10 Work Unit No. (TRAIS)** **11 Contract or Grant No.** C2107
12 Sponsoring Agency Name and Address Kansas Department of Transportation Bureau of Research 2300 SW Van Buren Topeka, Kansas 66611-1195		**13 Type of Report and Period Covered** Final Report August 2017–May 2020 **14 Sponsoring Agency Code** RE-0667-18
15 Supplementary Notes For more information write to address in block 9.		

16 Abstract

Critical shear stress is the stress exerted by flowing water that initiates soil erosion. It is a required parameter for estimating scour around structures. The current state of practice for estimating critical shear stress in cohesive soils is to assume a minimum value based on experiments with cohesionless, coarse-grained soils. The most accurate method for determining the critical shear stress is to directly measure it with a laboratory or in situ erosion device. Unfortunately, erosion testing requires highly specialized equipment not available to many Departments of Transportation. Therefore, the objective of this study was to develop an empirical equation for estimating the critical shear stress in cohesive soils with commonly measured geotechnical properties. This study is unique because electrical resistivity, a common near surface geophysical method that was previously correlated with soil erodibility, was used as a geotechnical property. A total of 26 scour critical bridges with cohesive soils were selected for this study; five soil samples were collected at 12 of the sites in K-TRAN: KSU-15-4. At least one soil sample was collected from the remaining 15 sites to broaden the soil erosion characteristics for model development. Erosion testing was performed in an Erosion Function Apparatus and 13 independent variables (geotechnical properties) were measured. Multiple variable screening criteria identified the percent passing the No. 200 sieve, liquid limit, and electrical resistivity as the statistically significant variables to predict critical shear stress. A probabilistic analysis was used to develop design factors selected by the engineer for implementing the model to predict abutment scour. Finally, the critical shear stress model was validated in a blind study using a bridge site selected by KDOT. This report presents the model development, design factors, study recommendations, and two examples for implementation.

17 Key Words Critical Shear Stress, Cohesive Soils, Abutment Scour, Erosion Control, Electrical Resistivity		**18 Distribution Statement** No restrictions. This document is available to the public through the National Technical Information Service www.ntis.gov.	
19 Security Classification (of this report) Unclassified	**20 Security Classification (of this page)** Unclassified	**21 No. of pages** 64	**22 Price**

Form DOT F 1700.7 (8-72)

This page intentionally left blank.

Predicting Critical Shear Stress of Fine-Grained Soils in Kansas

Final Report

Prepared by

Stacey Kulesza, Ph.D., P.E.
Md Zahidul Karim, Ph.D

Kansas State University Transportation Center

A Report on Research Sponsored by

THE KANSAS DEPARTMENT OF TRANSPORTATION
TOPEKA, KANSAS

and

KANSAS STATE UNIVERSITY TRANSPORTATION CENTER
MANHATTAN, KANSAS

January 2021

NOTICE

The authors and the state of Kansas do not endorse products or manufacturers. Trade and manufacturers names appear herein solely because they are considered essential to the object of this report.

This information is available in alternative accessible formats. To obtain an alternative format, contact the Office of Public Affairs, Kansas Department of Transportation, 700 SW Harrison, 2nd Floor – West Wing, Topeka, Kansas 66603-3745 or phone (785) 296-3585 (Voice) (TDD).

DISCLAIMER

The contents of this report reflect the views of the authors who are responsible for the facts and accuracy of the data presented herein. The contents do not necessarily reflect the views or the policies of the state of Kansas. This report does not constitute a standard, specification or regulation.

Abstract

Critical shear stress is the stress exerted by flowing water that initiates soil erosion. It is a required parameter for estimating scour around structures. The current state of practice for estimating critical shear stress in cohesive soils is to assume a minimum value based on experiments with cohesionless, coarse-grained soils. The most accurate method for determining the critical shear stress is to directly measure it with a laboratory or in situ erosion device. Unfortunately, erosion testing requires highly specialized equipment not available to many Departments of Transportation. Therefore, the objective of this study was to develop an empirical equation for estimating the critical shear stress in cohesive soils with commonly measured geotechnical properties. This study is unique because electrical resistivity, a common near surface geophysical method that was previously correlated with soil erodibility, was used as a geotechnical property. A total of 26 scour critical bridges with cohesive soils were selected for this study; five soil samples were collected at 12 of the sites in K-TRAN: KSU-15-4. At least one soil sample was collected from the remaining 15 sites to broaden the soil erosion characteristics for model development. Erosion testing was performed in an Erosion Function Apparatus and 13 independent variables (geotechnical properties) were measured. Multiple variable screening criteria identified the percent passing the No. 200 sieve, liquid limit, and electrical resistivity as the statistically significant variables to predict critical shear stress. A probabilistic analysis was used to develop design factors selected by the engineer for implementing the model to predict abutment scour. Finally, the critical shear stress model was validated in a blind study using a bridge site selected by KDOT. This report presents the model development, design factors, study recommendations, and two examples for implementation.

Acknowledgements

The authors would like to thank the Kansas Department of Transportation for funding the research described in this report. The authors thank the KDOT project monitor Bradford Rognlie (Bureau of Structures and Geotechnical Services), as well as Michael Orth and Luke Metheny (Bureau of Structures and Geotechnical Services) and James Brennan (Bureau of Construction and Materials). Finally, we appreciated the help of Ed Eneihen and Kevin Vaughn (Bureau of Structures and Geotechnical Services) for this assistance coordinating the drilling at each site and collecting soil samples in the field. Out of state samples were collected by the FHWA for a separate study. The authors would like to thank the FHWA for granting permission for use of these data in this study.

Table of Contents

List of Tables

List of Figures

This page intentionally left blank.

Chapter 1: Introduction

Accurately predicting bridge scour in cohesive soils remains a challenge. The current state of the practice for predicting scour uses the Federal Highway Administration (FHWA) Hydraulic Engineering Circular 18 (HEC-18), which includes a conceptual scour analysis framework (Arneson, Zevenbergen, Lagasse, & Clopper, 2012). The original empirical scour equations in HEC-18 were based on cohesionless coarse-grained soils and were a function of grain size. Grain size predicts scour in cohesionless/non-cemented coarse-grained soils with reasonable accuracy because gravity force is the only resistive force against scour (Shields, 1936; Briaud, Govindasamy, & Shafii, 2017). These equations are only applicable when median grain size is above 0.008 inches (Arneson et al., 2012). This results in over conservative scour estimates in cohesive soils where the median grain size is typically well below the 0.008-inch threshold. In cohesive soils, cohesion and adhesion due to inter-particle forces provide resistance against scour, in addition to the gravity force (Grabowski, Droppo, & Wharton, 2011). Erosion resistance in both cohesionless and cohesive soils are typically presented as a function of the critical shear stress.

Critical shear stress is the applied hydraulic shear stress at which surface soil erosion initiates (Partheniades, 1965; Hanson, Cook, & Simon, 1999; Utley & Wynn, 2008; Bernhardt et al., 2011). Critical shear stress is related to soil erosion rate using the excess shear stress equation such that:

$$\dot{E} = k_d(\tau - \tau_c) \qquad \textbf{Equation 1.1}$$

Where:

$\dot{E}$ = the erosion rate (ft/s),

k_d= the erodibility coefficient (ft^3/lb-s),

τ = the hydraulic shear stress (lb/ft^2), and

τ_c = is the critical shear stress (lb/ft^2) (Partheniades, 1965; Hanson et al., 1999).

Equations to determine scour depth in cohesive soils were developed as a function of critical shear stress; however, in situ or laboratory erosion testing was recommended over empirical equations to determine critical shear stress (Arneson et al., 2012). Indeed, erosion testing is the most accurate approach in cohesive soils, but it requires highly specialized equipment which

many transportation agencies do not own, likely making this cost prohibitive. Therefore, the minimum median grain size for the given equation (developed for cohesionless soils) is often used for estimating scour in cohesive soils, leading to over conservative designs.

Several empirical equations have been developed to calculate critical shear stress in cohesive soils; however, these are rarely used in practice and none of the following equations were developed for bridge scour. Erosion in cohesive soils is affected by various physical, biological, and geochemical properties (Grabowski et al., 2011; Paterson, 1997). The relative contributions and interaction of these factors are still unknown and there has been no research to date investigating all of these factors in one empirical model, likely due to large number of parameters. One of the earliest empirical equations for critical shear stress (τ_c) was developed by Dunn (1959).

$$\boldsymbol{\tau_c = 0.01(\tau_s + 180)\tan(30 + 1.73PI)} \qquad \textbf{Equation 1.2}$$

Where:

τ_s (lb/ft^2) = the undrained shear strength, and

PI = the plasticity index of soil.

Dunn (1959) developed this equation based on linear regression of multiple geotechnical properties. The equation was developed for the design of earth lined canals and the soil samples in the study had an average plasticity index (PI) of 12, which is below the average PI of the soils in this study (average PI of 22). Over half of the 46 soil samples from the lined canals were silt or silty sands with lower PI. Kimiaghalam, Clark, and Ahmari (2015) also correlated critical shear stress and shear strength parameters, specifically cohesion, but the empirical model was based on only 13 soil samples at a narrow range of critical shear stress (i.e., 0.006–0.21 psf). Amos, Feeney, Sutherland, and Luternauer (1997) studied the erosion mechanism of river delta sediments and developed an equation as a function of bulk density. These sediments were collected from the river bottom and were very loose, unlike the samples collected from river banks in this study. Therefore, the Amos et al. (1997) relationship was based on measured critical shear stress ranging from 0.002 to 0.01 psf. This is well below the typical critical shear stress range in cohesive soils (Arneson et al., 2012). Thoman & Niezgoda (2008) were one of the few studies that included both geotechnical and geochemical properties. They used 25 soil samples collected from five different creek beds in northeast Wyoming and they found that activity of clay (CA), dry density (ρ_d), specific gravity

(G_s), hydrogen ion concentration (pH), and water content (w) were significant soil properties affecting critical shear stress such that:

$$\tau_c = 77.28 + 2.20(CA) + 0.26\rho_d - 13.49G_s - 6.4pH + 0.12w. \quad \textbf{Equation 1.3}$$

Similar to Amos et al. (1997), the critical shear stresses of the sediment beds were very low (i.e., range 0.002 to 0.32 psf) compared to the measured critical shear stresses of the river bank materials in this study (0.008 to 2.02 psf). More recently, Mahalder, Schwartz, Palomino, and Zirkle (2018) developed four sets of equations based on physiographic regions. Despite the complexity of the empirical equations, all four equation sets had poor correlation.

Many other equations to predict critical shear stress based on geochemical or biological properties alone (as opposed to engineering properties) have also been developed. Classic examples include Ariathurai and Arulanandan (1978), who showed critical shear stress increases with increasing cation exchange capacity. Arulanandan (1975) showed that critical shear stress decreases with increasing sodium absorption ratio. On the biological side, burrowing organisms create water filled chambers in consolidated sediment resulting in higher water content, lower shear strength and lower critical shear stress (Widdows, Brinsley, & Pope, 2009). Similar to many of the engineering equations, these geochemical and biological equations focused on riverbed sediments at very low critical shear stresses. Note that although these are likely not all of the empirical equations to predict critical shear stress, researchers have selected different properties for their empirical models and there is no consensus on what controls the onset of cohesive soil erosion.

Shan, Shen, Kilgore, and Kerenyi (2015) developed an empirical equation for predicting the critical shear stress in cohesive soils, specifically for the HEC-18 cohesive soil bridge scour equations. Shan et al. (2015) found percent fines, water content, plasticity index, and unconfined compressive strength as statistically significant model variables, all of which are commonly measured by transportation agencies. Therefore, this equation allows transportation agencies to estimate critical shear stress without conducting site specific testing; however, the equation is only applicable for shear stress ranging from 0.06 to 0.31 psf. Furthermore, the model was based upon laboratory-prepared soils with plasticity index ranging from 4 to 25, liquid limit between 15 to 50,

and percent fines ranging from 10 to 90. These soils and lower shear stresses were likely chosen to focus on the worst case (i.e., more erodible) cohesive sediment in riverbeds (i.e., primarily pier and contraction scour).

Briaud, Shafii, Chen, and Medina-Cetina (2019) conducted a robust analysis of the erodibility of all soils using three common erosion devices. Briaud et al. (2019) presented several methods to estimate soil erodibility including a "quick" method based on soil classification and empirical models developed with the same soil properties considered in this study to predict different erosion parameters. One of these erosion parameters included the critical shear stress of fine-grained soils using an erosion function apparatus (EFA). They identified total unit weight, water content, undrained shear strength measured with a miniature vane shear device, percent passing the No. 200 sieve, median particle size, and activity (the ratio of plasticity index to percent clay) as significant variables. Although a similar process was used for this study, the final model is simpler with only three variables. There are likely fewer variables in this study because multicollinearity, or the interdependence of variables amongst each other, was used as a variable screening tool. This specifically eliminated including both percent passing the No. 200 sieve and median particle size, even though both were found to be statistically significant. Also, the two models focus on slightly different soil classifications (i.e., cohesive versus fine grained), potentially resulting in different statistically significant variables. In this study the focus was on all soils with cohesion to align with Shan et al. (2015) as their model was specifically developed to be incorporated in the HEC-18 bridge scour design process. This proposed model also includes a geophysical measurement, electrical resistivity, as a model variable which was not considered by Briaud et al. (2019). Electrical resistivity is a bulk soil property that incorporates many of the physical, geochemical, and biological properties that previous researchers identified to influence critical shear stress separately. Therefore, electrical resistivity may be considered as dimensionality reduction, meaning electrical resistivity may capture these interactions and convert them to a single property.

The focus of this study was abutment scour which is due to the obstruction of flow by the abutment and roadway embankment and does not occur in the riverbed (Arneson et al., 2012). Tucker-Kulesza and Karim (2017) identified that most measured soil properties and applied

hydraulic shear stresses in a previous KDOT study, K-TRAN: KSU-15-4, were outside of the limits of the Shan et al. (2015) model. Therefore, although Shan et al. (2015) and Briaud et al. (2019) are improvements over previous equations based on coarse-grained soils, there is still a need for calculating critical shear stress with a simple model, outside of riverbeds where a wider range of cohesive soil properties were observed, and where hydraulic stresses may be higher.

Karim and Tucker-Kulesza (2018) established that electrical resistivity tomography (ERT) can be used to rapidly characterize the erosion potential of a bridge site, primarily for prioritizing bridges for more advanced scour analyses. ERT is considered one of the Advanced Geotechnical Methods in Exploration by the FHWA for its capacity to obtain continuous subsurface data between soil borings (FHWA, 2020). In addition to site characterization, researchers have correlated electrical resistivity with geotechnical properties to reduce the number of geotechnical tests in a project (e.g., Kouchaki, Bernhardt-Barry, Wood, & Moody, 2018; Kibria & Hossain, 2012; Abu-Hassanein, Benson, & Blotz, 1996; Ahmed, Hossain, & Khan, 2018; Chen, Wei, Irfan, Xu, & Yang). Karim and Tucker-Kulesza (2018) recommended ERT because of the overlap between physical, geochemical, and biological properties that affect both soil erodibility and electrical resistivity. Tucker-Kulesza and Karim (2017) noted that there was a direct correlation between electrical resistivity and critical shear stress in cohesive soils; however, the relationship was not strong ($R^2 = 0.52$). Still, an advantage of electrical resistivity is that it is an intrinsic soil property which is influenced by non-engineering properties that also control soil behavior, like geochemical and biological factors (Friedman, 2005).

Previous equations to calculate critical shear stress were limited because they did not consider the combined effects of physical, geochemical, and biological factors. This is likely because there are too many variables that may influence cohesive soil erosion identified in the literature, making the analysis too complicated and an unreasonable scope. This study included electrical resistivity as a soil property because it inherently includes the influence of geochemical and biological conditions in the measurement. For example, electrical resistivity will decrease with increasing cation exchange capacity (Kibria, 2014) and increase as the percentage of calcium ions increases (Kibria & Hossain, 2012). Chambers created by burrowing organisms will decrease the electrical resistivity due to increased saturation in the chambers (Widdows et al., 2009; Kouchaki

et al., 2018). Thus, both geochemical and biological factors are captured by electrical resistivity without additional experiments for each factor. Including electrical resistivity as a soil property is one unique aspect of this study. As will be shown, electrical resistivity was one of the three significant variables for calculating critical shear stress.

The objective of this study was to develop an empirical equation for estimating the critical shear stress in cohesive soils with commonly measured geotechnical properties. There are five chapters in this report detailing the process by which the objective was achieved. Following this introduction, Chapter 2 includes a brief literature review of different soil erosion testing methods and electrical resistivity imaging. Chapter 3 describes the methodology of this research including the field work, model development, and the probabilistic analysis. It is followed by Chapter 4 where the final model, design factors, and validation of this study are provided. Conclusions, recommendations for implementation, and future work are discussed in the final chapter. Two design examples are included in Appendix A.

Chapter 2: Literature Review

2.1 Soil Erosion

Erosion is the process of soil loss due to water flow. Erosion occurs when exerted shear forces by the flowing water overcome the resistive forces within the soil mass. The resistive forces from the soil include gravity, friction, cohesion, and adhesion depending on the type of soil (Leeder, 1999; Winterwerp & van Kesteren, 2004). This threshold for erosion can be measured in terms of critical shear stress. The process of erosion initiates once the shear stress exerted by the flowing water exceeds the critical shear stress of the soil. After this critical point, if flow continues, the amount of soil eroded per unit time is defined as the erodibility or erosion rate.

Cohesionless soils erode as individual particles while cohesive and cemented soils erode as blocks. As described in the introduction, the resistance against erosion in cohesionless soils is controlled by the weight of soil (i.e., particle size). Inter-particular forces such as cohesion and adhesion provide the resistance against erosion in addition to the weight of soil in cohesive soils (Grabowski et al., 2011). The critical shear stress, τ_c, in Equation 2.1 is the shear stress exerted by flowing water on the soil surface that initiates erosion. Any hydraulic stress below the critical shear stress will not cause the soil to erode. In cohesionless soils, only the weight of the soil resists the hydraulic stress. Shield's (1936) equation is the classic relationship between critical shear stress and particle size developed for cohesionless soils such that:

$$\boldsymbol{\tau_c = K_s(\rho_s - \rho_w)gd} \qquad \textbf{Equation 2.1}$$

Where:
K_s = the dimensionless Shield's parameter based on soil type,
ρ_s = the particle mass density (slugs/ft^3),
ρ_w = the mass density of water (1.94 slugs/ft^3),
g = gravitational acceleration (32.2 ft/s^2), and
d = the particle size (ft) (Shields, 1936).

Studies have shown that relationships based on particle size underestimate critical shear stress in cohesive soils, thus overestimating the amount of erosion (Hanson & Simon, 2001). The summary of equations to predict critical shear stress in the introduction highlight that there is not consensus on the measurable properties that control critical shear stress in cohesive soils. Also,

most previous studies have focused on sediments in riverbeds, where much lower critical shear stress were observed compared to the measured critical shear stress near bridge abutments which were the soils of interest in this study.

2.1.1 Properties that Affect Cohesive Soil Erosion

Many researchers have developed empirical relationships between critical shear stress and erodibility for cohesive soils based on laboratory tests. In addition to those presented in the introduction, common geotechnical parameters such as clay content (Panagiotopoulos, Voulgaris, & Collins, 1997; van Ledden, van Kesteren, & Winterwerp, 2004; Winterwerp & van Kesteren, 2004; Houwing, 1999; Dickhudt, Friedrichs, & Sanford, 2011; Debnath, Nikora, Aberle, Westrich, & Muste, 2007) and bulk density (Jepsen, Roberts, & Lick, 1997; Lick & McNeil, 2001; Amos et al., 2004; Bale, Stephens, & Harris, 2007) have been correlated with critical shear stress. Researchers have also related plasticity index (Smerdon & Beasley, 1961; Dunn, 1959) and the liquidity index to soil erosion (Amaryan, 1993; Bale et al., 2007). All variables included in this study were previously identified as a soil property that impacts cohesive soil erosion, including electrical resistivity (Karim & Tucker-Kulesza, 2018; Karim, Tucker-Kulesza, & Bernhardt-Barry, 2019). Despite the wealth of research, critical shear stress is governed by the inter-particular forces and the chemistry between pore-water and flowing water. These are site-specific properties and are very difficult to estimate in the laboratory (Heinzen, 1976; Grissinger, 1982; Knapen, Poesen, Govers, Gyssels, & Nachtergaele, 2007). Electrical resistivity, specifically ERT measured in the field, captures these inter-particle forces, geochemical properties, and biological properties that are difficult to measure in a laboratory setting.

2.2 Erosion Function Apparatus

Because no unifying equation exists based on measurable soil properties to predict cohesive soil erosion, researchers have developed devices to directly measure the erodibility of soils. These devices can be divided into four categories: rotating apparatus tests; JET erosion tests; flume style erosion tests; and pinhole erosion tests. Each of these devices imparts a different hydraulic loading mechanism, or the way the water flows across the soil sample. The Erosion Function Apparatus (EFA) is a simple flume style test that was used exclusively in this research.

In an EFA test, soil samples collected in ASTM standard Shelby tubes are mounted in the flume as shown in Figure 2.1. Water is pumped at different velocities within a 4.4-ft-long rectangular flume that has a cross-sectional dimension of 4 in. × 2 in. The velocity of water flow in the rectangular flume is maintained using a flow control pump. The average flow velocity range is 0.32 to 19.6 ft/s.

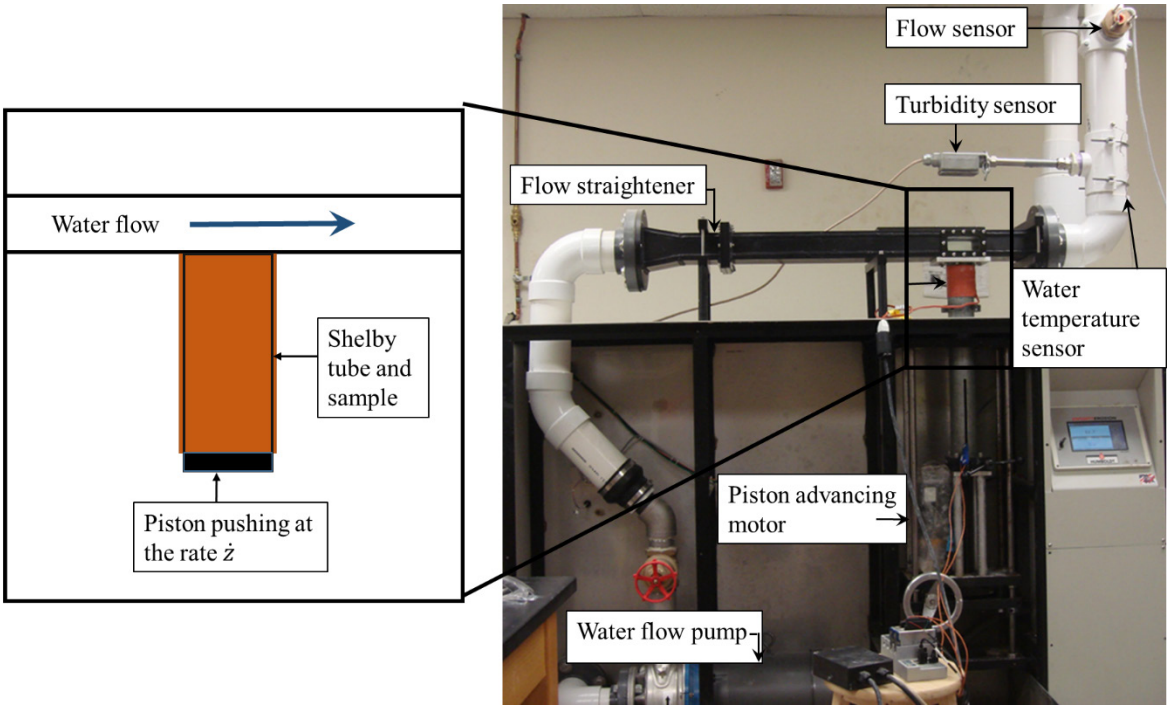

Figure 2.1: Erosion function apparatus at K-State

EFA tests are conducted on soils at their in-situ water content. During the test, the bottom of the sample is placed over the piston and the top is kept flush with the base of the rectangular flume. At first, the sample is eroded under the minimum velocity (typically 1.64 ft/s) for one hour. When the sample erodes, the piston is pushed upward to keep the soil flush with the bottom of the flume. The sample is visually inspected during testing to determine when to extrude the sample and how much. The amount of sample eroded is equal to the length of sample lifted by the piston. This procedure is repeated for at least six different flow velocities so the erosion rate in inches per hour is obtained for each velocity. The objective of erosion tests in an EFA is to obtain the plot of erosion rate, $\dot{z}$, in./hr versus shear stress, τ, psf. The erosion rate, $\dot{z}$, is:

$$\dot{z} = \frac{h}{t}$$ **Equation 2.2**

Where:

h = the length of sample eroded in inches, and

t = the duration of the test.

The Moody (1944) chart is used to calculate the shear stress, τ, as:

$$\tau = \frac{1}{8}\alpha f \rho V^2$$ **Equation 2.3**

Where:

f = the friction factor obtained from the Moody chart,

α = the unit conversion constant,

ρ = the density of water (slugs/ft^3), and

V = the mean velocity of flow in the pipe (ft/s).

Additional details regarding EFA testing, including determining the friction factor are discussed in Tucker-Kulesza and Karim (2017).

2.3 Electrical Resistivity

Electrical resistivity is a common geophysical measurement that can be obtained in the field or in the laboratory. An electric current I (measured in amperes) is injected into the soil through current electrodes and resulting voltage potential V (measured in volts) is measured across another pair of electrodes. The fundamentals of field electrical resistivity, ERT, were described in a previous KDOT study where ERT was used to characterize the corrosion potential of aggregates in mechanically stabilized earth walls (Tucker-Kulesza, Snapp, & Koehn, 2016). Details regarding laboratory-measured electrical resistivity, which is commonly used by Departments of Transportation for characterizing the corrosion potential of backfill for mechanically stabilized earth walls, are included herein in the methods. Regardless of the measurement technique, the properties that affect electrical resistivity are the same.

2.3.1 Properties that Affect Electrical Resistivity

Soil characteristics such as water content and saturation, porosity, permeability, mineralogy, clay content, and temperature affect electrical resistivity measurements (Zonge, Wynn, & Urquhart, 2005). Electrical current in soil is dependent on the displacement of ions in pore-water; therefore,

water content and saturation are the primary factors that influence soil electrical resistivity (Kibria & Hossain, 2012; McCarter, 1984). Electrical resistivity is also dependent on the electrical charge density at the surface of the solid constituents. The inherent higher electrical charges associated with clay particles result in lower resistivity than coarse-grained soils (Fukue, Minato, Horibe, & Taya, 1999). Coarse-grained soils and aggregates typically have higher electrical resistivity due to the presence of larger voids where the current dissipates.

2.4 Model Development

The objective of this study was to develop a model, or equation, to predict the critical shear stress in cohesive soils using measurable soil properties. Typical linear regression involves measuring several independent variables and selecting them for regression based on the individual goodness of fit with the desired dependent variable. A different process was used in this study to select the variables and then to confirm selection before regression. All soil properties measured in this study were previously identified as variables that impact cohesive soil erodibility (e.g., Grabowski et al., 2011; Kimiaghalam et al., 2015; Karim & Tucker-Kulesza, 2018; Arneson et al., 2012). Some of these properties measure similar soil characteristics leading to multicollinearity in the dataset. Multicollinearity is the existence of near-linear to linear relationship between a pair of independent variables, and it can cause the regression coefficients to be misleading and reduce the model predictability (Mendenhall & Sincich, 2012). Multicollinearity has been used for variable screening in other civil engineering applications, such as hydrologic linear regression models (Yoo & Cho, 2019; Campos-Aranda, 2011). Multicollinearity can reduce the statistical power of a model, meaning variables identified as statistically significant may not be significant. Also, multicollinearity can cause the model coefficients to be too sensitive to the independent variables. This means that the model may not accurately predict the dependent variable when data not from the original dataset are used. Multicollinearity is measured by the coefficient correlation, r (dimensionless ratio) such that:

$$r = \frac{\sum_i (x_{1i} - \bar{x}_1)(x_{2i} - \bar{x}_2)}{\sqrt{\sum_i (x_{1i} - \bar{x}_1)^2 \sum_i (x_{2i} - \bar{x}_2)^2}}$$ **Equation 2.4**

Where:

-1≤ r ≤1; x_{1i} and x_{2i} are the two variables between which r is being measured for the i-th observation (Mendenhall & Sincich, 2012).

A positive r denotes that the pair of variables are positively related (increasing one increases the other) and vice versa. The closer the $|r|$ value is to 1, the stronger the multicollinearity between the two independent variables.

The backward elimination technique is one of the most widely used variable screening techniques for linear regression (Mendenhall & Sincich, 2012). Backward elimination is a stepwise regression which identifies the optimum number of independent variables to be used in a model. The predictive performance of a variable is evaluated in successive iterations based on the t-statistic and removed if not satisfactory until all the variables existing in the model have a significant t-statistic (Mendenhall & Sincich, 2012). Therefore, backward elimination verifies that all model variables and the combination of the model variables are statistically significant. Similarly, the F score method identifies the most influential independent variables on a dependent variable (Pedregosa et al., 2011). In this method, independent variables are ranked based on their F scores such that:

$$F = \frac{r^2(n-2)}{1-r^2}$$ **Equation 2.5**

Where:

r = the correlation coefficient for a certain independent variable, and

n = the total number of observations.

F scores are commonly used for feature (variable) selection in machine learning applications to reduce overfitting of data and improve model accuracy.

Chapter 3: Methodology

Ultimately 26 sites were used to develop this model. Twelve of the sites were from a previous KDOT study (Tucker-Kulesza & Karim, 2017). Ten of the sites were selected by KDOT for this study with a goal of collecting more high erodibility and low erodibility samples compared to Tucker-Kulesza and Karim (2017). One additional site in Kansas was selected by KDOT and the three remaining sites were from out of Kansas. These four sites were for a separate FHWA study and were included in the model development. Therefore, most of the samples (i.e., 67 of 70) were collected from the 23 sites in eastern Kansas selected by KDOT based on scour vulnerability. As expected, 20 of the Kansas sites characterized as alluvium geology meaning they were deposited relatively recently by streams on their floodplain or delta (Kansas Geological Survey, n.d.). Two of the sites were Dakota formation, characterized by white, gray, red, brown, and tan kaolinitic claystone, mudstone, shale siltstone, and interbedded and lenticular sandstones (Zeller, 1968). The remaining Kansas site was formed by glacial drift. Glacial drift sediment was transported by glaciers and deposited directly on land (Neuendorf, Mehl, & Jackson, 2011). A map of the 23 Kansas sites is shown in Figure 3.1 along with their surficial geology. The remaining three soil samples were collected from Ohio, Nebraska, and Colorado by the FHWA. These samples were included because adding them to the model did not change the statistically significant variables or the final linear regression. Therefore, they highlight that the model is not limited to eastern Kansas.

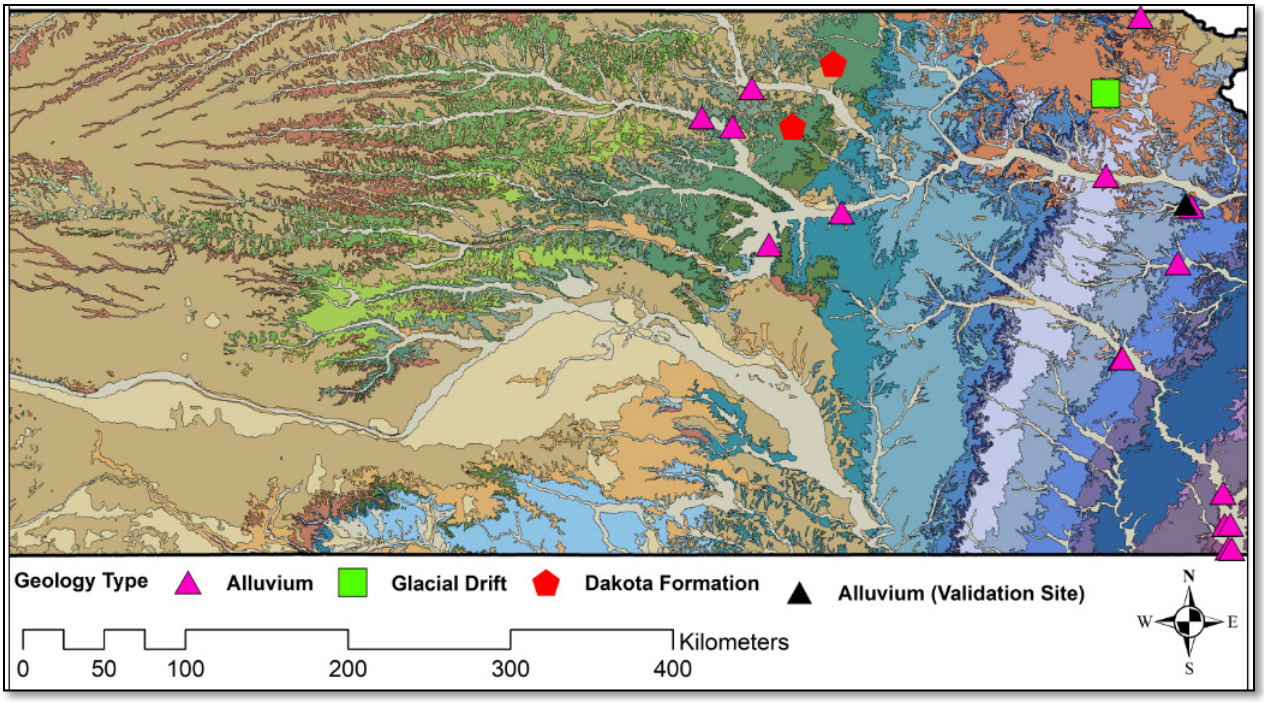

Figure 3.1: Location of the 23 sites from eastern Kansas

3.1 Soil Sampling

Thin-walled Shelby tubes were used following ASTM standard D1587 (2015) to collect soil samples at each bridge site. Most of the samples were from Tucker-Kulesza and Karim (2017). Tucker-Kulesza and Karim (2017) collected up to five 3.5-inch, 2-ft-long samples at each site at a fixed drilling position. The top foot of soil was augered through to remove the surface vegetation. As a result, the total drilling depth for five samples was typically 11 feet. Drilling was performed as close to the stream as possible and at least 30 feet from the pavement shoulder or the bridge abutment so that collected sample represented the native geology of the site, avoiding influence from the bridge on the measured resistivity. Drilling was not conducted in the streambeds as this study focused on abutment scour. The Shelby tubes were pushed using the drill rig without rotation to the desired depth. Two samples were collected from the 10 new Kansas sites selected for this study at a desired depth following the same protocol. One sample was used for EFA testing and soil classification. The second sample was used for shear strength testing. Additional undisturbed samples were collected from the original 12 sites in Tucker-Kulesza and Karim (2017) at a desired depth to provide undisturbed samples for shear strength testing for model development. The four

FHWA samples were 3.5 inches and 3 ft long. These samples were cut in half prior to testing. One half was used for EFA testing directly in the Shelby tube and classification. The other half was extruded and trimmed for strength testing. ASTM standard D4220 (2014) was followed for preserving and transporting soil samples to maintain the in-situ conditions. Samples were stored in a 100% humidity-controlled room until testing.

3.2 ERT Surveys

ERT surveys were conducted on the same day of soil sampling at each Kansas site. ERT typically utilizes four electrodes: two current electrodes, and two voltage electrodes. The current electrodes (A, B) create an electric field within the subsurface from an external direct current source while the voltage electrodes (P, Q) measure the voltage potential between two subsurface points. For a measured voltage potential and an induced current, the apparent resistivity, ρ_a (Ωm), is obtained using:

$$\boldsymbol{\rho_a = \left(\frac{2\pi V_{PQ}}{I}\right)\left[\frac{1}{r_{AP}} - \frac{1}{r_{AQ}} - \frac{1}{r_{BP}} + \frac{1}{r_{BQ}}\right]^{-1}} \qquad \textbf{Equation 3.1}$$

Where:
I = the electric current (amperes),
V = the voltage potential (volts),
r = the lateral distance between respective electrodes (m), and
A/B/P/Q represent electrodes used for current or voltage measurements.

Note that the term “apparent” is used because ERT measurements assume the entire subsurface is homogenous (Everett, 2013).

More than four electrodes can be used in ERT surveys to reduce data collection time and cover a larger area. ERT in this study was set up to meet two criteria: depth of penetration and data resolution. The setup had to be such that resistivity signal could penetrate beyond the maximum borehole depth of 11 feet. High lateral resolution was required for constructing the two-dimensional (2-D) soil erodibility profile in Tucker-Kulesza and Karim (2017). Tucker-Kulesza and Karim (2017) identified the dipole-dipole array as the best configuration to use for these criteria. The dipole-dipole array also minimizes coupling effects (an electric link between the current and voltage pairs), compared to other arrays (Binley & Kemna, 2005) resulting in less

noisy data. In the dipole-dipole array, the spacings between the current electrodes (A, B) and the voltage electrodes (P, Q) remain constant (a); however, the spacing between the current electrode pair and voltage electrode pair, na is variable (Figure 3.2). Note that as n increases, the depth to the measured apparent resistivity point also increases.

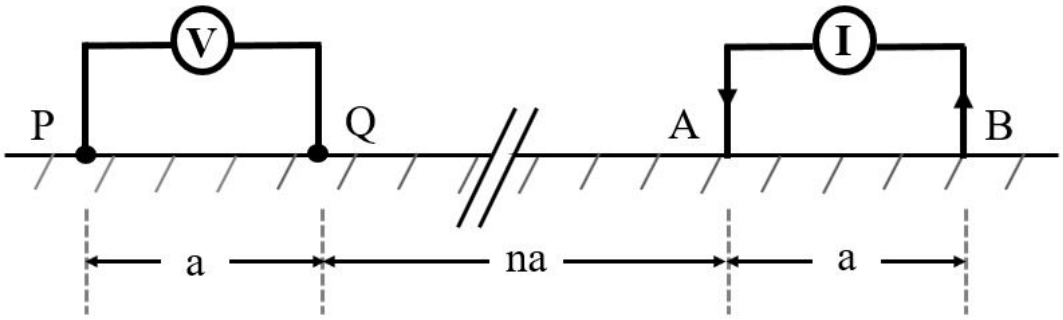

Figure 3.2: Schematic demonstrating the dipole-dipole array

The AGI SuperSting R8/IP multichannel imaging system was used with 56 electrodes for data acquisition. Electrodes were spaced at a uniform 1.5 ft, resulting in an 82.5-ft-long survey. Because most data points were in the central region of an ERT survey line using a dipole-dipole array, and because the best resolution was obtained in that region, the survey line was oriented so that the sampling borehole was located between the 28th and 29th electrodes. Visible sources of cultural noise (e.g., utilities, power lines, fiber optic cables, cell phone towers) were avoided near the survey line. The data collection for each ERT survey took about 30 minutes at each site. All resistivity data were processed with AGI *EarthImager 2D* software (Advanced Geosciences, Inc., 2009). Details regarding data inversion are in Tucker-Kulesza and Karim (2017). Figure 3.3 shows ERT data acquisition at a site. The borehole was located between the two flags and drilled after the ERT survey was complete.

Figure 3.3: Field ERT data acquisition system, flags indicate where boreholes will be located

The final inverted resistivity section was approximately 82.5 × 22 ft^2. This inverted section is actually a contour plot of resistivity with over 45,000 elements of a finite-element mesh. As mentioned, each sample for erosion testing was 1.3 ft long with a diameter of 3.5 inches (0.3 ft). The projected area of 1.3 × 0.3 square feet contained 16 elements of the resistivity mesh in the 2-D section. The average resistivity of these 16 elements was assigned as the resistivity for that soil sample. Because dipole-dipole array data are sensitive to near surface heterogeneity, a sensitivity analysis was conducted on the mesh discretization. The default mesh of two elements between electrodes was increased to six per 1.5 ft (electrode spacing) to reduce the likelihood of mathematical artifacts. Further discretization of the mesh did not improve the quality of the inversion (Karim, 2016).

3.3 Laboratory Resistivity Measurements

Karim et al. (2019) showed that laboratory resistivity measurements provide statistically similar resistivity values as in situ ERT. The laboratory resistivity measurements were used for the non-Kansas samples where ERT testing was not possible. A Nilsson Resistance Meter Model 400 was used for the laboratory resistivity measurements. An M.C. Miller Large Soil Box (16.5 $in.^3$) was used to hold the soil specimen at the in-situ density. As shown in Figure 3.4, the resistance

meter was attached to the four electrodes in the soil box. The outer two electrodes are the current electrode pair and the inner electrode pair measures the voltage potential. The soil resistance is directly measured in a soil box and converted to the resistivity based on the box dimensions, known as a box factor. The cross-sectional area and the distance between the voltage electrodes of the soil box used in this study were such that the resistivity (Ωcm) was the same as the measured resistance (Ω) from the resistance meter. Each specimen was compacted into three equal layers following ASTM G187 (2018) to fit within the soil box at the in-situ density and water content and verified by phase relationships. The laboratory resistivity reading was then measured, and the soil temperature was recorded. Although it is the author's recommendation that ERT be used to measure electrical resistivity, soil boxes such as the one shown in Figure 3.4 provide an affordable alternative provided the sample is reconstituted at the in-situ density and water content. KDOT uses soil boxes to measure the corrosion potential of mechanically stabilized earth wall backfill (Tucker-Kulesza et al., 2016; Brady, Parsons, & Han, 2016), therefore this equipment is currently available.

Figure 3.4: Soil box for laboratory resistivity measurements

3.4 Erosion Testing and Soil Properties Measurements

The soil erosion rate was measured in the EFA as described in Tucker-Kulesza and Karim (2017). The Shelby tube was cut to remove the holes that connect to the drill head, and

approximately 1.3 ft of soil was used for the erosion test. The erosion rate was measured at six different water velocities for each sample. The shear stress due to the flowing water that caused the erosion was calculated using Equation 2.3. A plot of shear stress versus erosion rate was created for each sample. An example plot is shown in Figure 3.5 for US-73. The critical shear stress was taken as the stress at which 0.004 inch/hr (0.1 mm/hr) erosion occurs based on the recommendation of Briaud et al. (2017). The critical shear stress for US-73 was 0.301 psf.

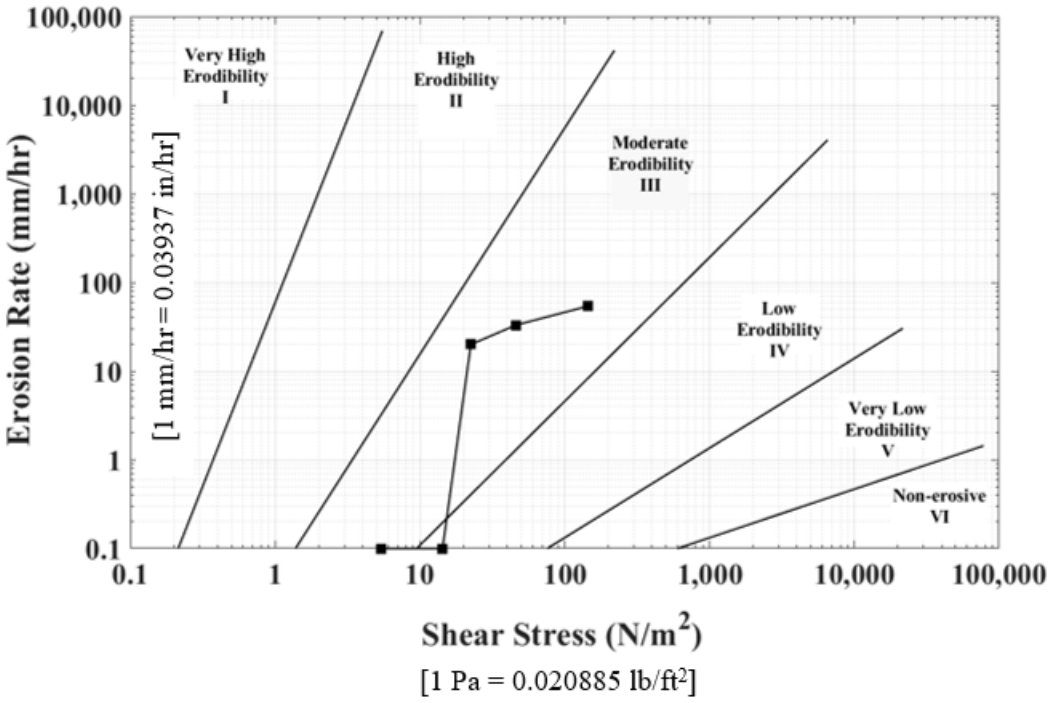

Figure 3.5: Example erosion test results for US-73

The remaining 0.7 ft soil was used for determining various soil properties. Additional soil property measurements included: water content (ASTM D2216, 2019), Atterberg limits (ASTM D4318, 2017), grain size distribution (ASTM D7928, 2017; ASTM C117, 2017; ASTM C136, 2014), and bulk density (ASTM D7263, 2018). Dry density, void ratio, porosity, and degree of saturation were calculated based on the measured properties. The additional undisturbed soil sample collected at each site was used for triaxial unconsolidated undrained shear strength testing (ASTM D2850, 2015).

3.5 Model Development

The electrical resistivity and laboratory measured soil properties were used as dependent variables for the linear regression. The critical shear stress from the EFA test was used as the independent variable for linear regression. Multicollinearity analysis was first used to reduce the number of variables in the model. Final variables were selected using the backward elimination technique and *F* score analysis. A multiple linear regression analysis was run based on the selected variables to calculate the critical shear stress. The results of the multiple linear regression were finalized by checking the model coefficients using the "leave one out" method and comparing the results to the original model. Finally, a design factor, α_d, was created to minimize the probability of over predicting the design critical shear stress when the model is used for estimating the critical shear stress to predict abutment scour following the equations for cohesive soils in the HEC-18 (Arneson et al., 2012).

Chapter 4: Results and Analysis

The erosion test results used to determine the critical shear stress are shown in Figure 4.1 with the USCS classification for each sample. The critical shear stresses of these samples varied between 0.008 and 2.03 psf. Measured critical shear stresses are shown using asterisks along the x-axis in Figure 4.1. The critical shear stress of the 70 samples in this study ranged across four (out of six) different categories of erodibility. Most of the measured critical shear stress was between 0.21 and 1.46 psf. Critical shear stresses in this range are considered "low erodibility" according to Arneson et al. (2012).

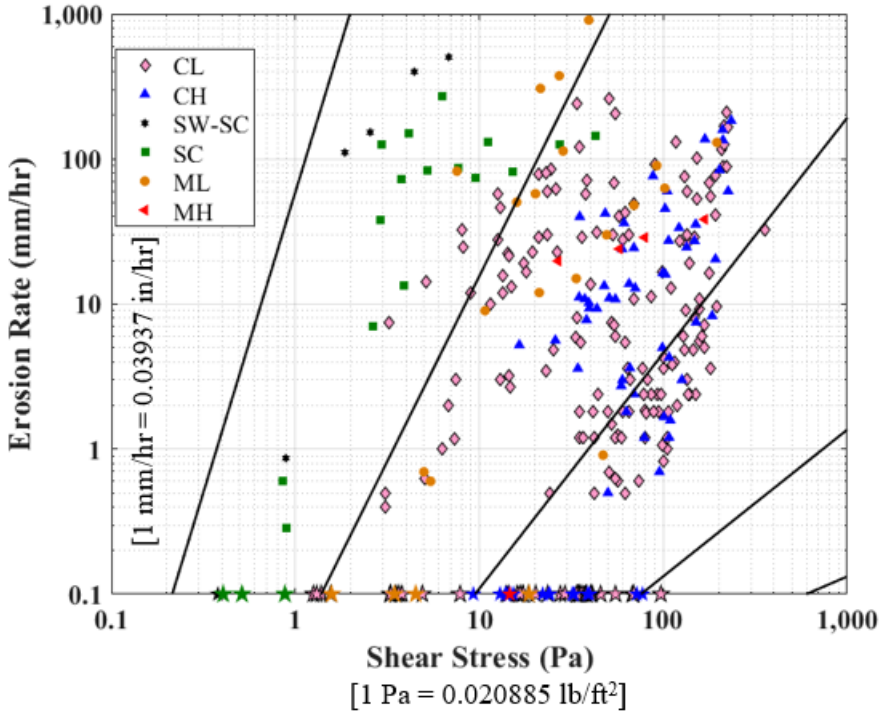

Figure 4.1: EFA results with USCS classification for the 70 samples

The range, minimum, maximum, mean, median, and standard deviation of critical shear stress (dependent variable) and 13 other soil properties (independent variables) for all 70 samples are shown in Table 4.1. Variable transformation using an appropriate function is the first step in multiple linear regression to reduce the skewness in the distribution of the variables (Mendenhall & Sincich, 2012). Logarithmic transformation was used to reduce the skewness in the critical shear stress, electrical resistivity, median grain size, and percent fines. Logarithmic transformation was

used for these four variables because of the difference between the mean and median values as well as the relatively large standard deviation compared to the range. The difference between mean and median for the remaining variables were small; hence, no transformation was needed.

Table 4.1: Observed variable statistical descriptions

Variable	Range	Min.	Max.	Mean	Median	Std. Dev.
Critical shear stress, $\boldsymbol{\tau_c}$ (lb/ft^2)	2.02	0.008	2.03	0.49	0.36	0.43
Electrical resistivity, $\boldsymbol{\rho}$ ($\boldsymbol{\Omega}$m)	321.7	6.0	327.7	28.87	12.71	54.90
Water content, $\boldsymbol{w}$ (%)	29	11	40	26.77	27.08	4.74
Percent fines, $\boldsymbol{f}$ (%)	89	11	100	90.30	96.79	19.21
Median grain size, $\boldsymbol{d_{50}}$ (in)	0.07554	0.00005	0.07559	0.00354	0.00040	0.01428
Liquid limit, $\boldsymbol{LL}$ (%)	54	26	80	42.72	41.50	10.25
Plastic limit, $\boldsymbol{PL}$ (%)	24	10	34	20.52	20.00	4.18
Plasticity index, $\boldsymbol{PI}$ (%)	49	3	52	22.20	22.00	10.01
Void ratio, $\boldsymbol{e}$ (dimensionless)	0.90	0.28	1.18	0.77	0.76	0.19
Porosity, $\boldsymbol{n}$ (dimensionless)	0.32	0.22	0.54	0.43	0.43	0.06
Degree of saturation, $\boldsymbol{S}$ (%)	32	67	100	90.90	90.58	6.53
Bulk density, $\boldsymbol{D_b}$ (lb/ft^3)	36.0	109.0	145.0	120.34	119.52	6.84
Dry density, $\boldsymbol{D_d}$ (lb/ft^3)	53.7	77.8	131.5	95.94	95.59	10.27
Undrained strength, $\boldsymbol{S_u}$ (lb/ft^2)	4709	291.2	5000	2037	2000	992.2

Thirteen properties were measured for each sample, 12 geotechnical properties and one geophysical property (i.e., electrical resistivity). All measured properties were previously identified as variables that impact cohesive soil erodibility (e.g., Grabowski et al., 2011; Kimiaghalam et al., 2015; Karim & Tucker-Kulesza, 2018; Arneson et al., 2012). Note that soils with at least 10% fines are considered cohesive (Mitchell & Soga, 2005). As shown in Table 4.1, the minimum percent fines in this study was 11 percent (although the mean was 90.3%). Some of the geotechnical properties inherently measure similar soil characteristics, which may cause multicollinearity in the dataset. Therefore, multicollinearity was evaluated to identify the independent variables based on the r values (Equation 2.4), shown in Table 4.2. Three sets of variables were found to be dependent on each other: percent fines (f) and median grain size (D_{50}, both shown in orange); the Atterberg limits (LL, PL, PI, shown in green); and void ratio (e), porosity (n), total unit weight (γ), and dry unit weight (γ_d, all shown in blue). The red squares show where the variable overlaps on both axes, hence a 1:1 relationship.

Table 4.1: Multicollinearity *r* values

	f	D_{50}	LL	PL	PI	ρ	w	e	n	S	γ	γ_d	s_u
f	1.00	0.89	0.49	0.11	0.45	-0.76	0.40	0.12	0.11	0.05	-0.07	-0.09	-0.11
D_{50}	-0.89	1.00	-0.71	-0.14	-0.66	0.82	-0.37	-0.19	-0.17	-0.16	0.09	0.15	-0.02
LL	0.49	-0.71	1.00	0.24	0.91	-0.62	0.52	0.38	0.36	0.27	-0.25	-0.34	-0.07
PL	0.11	-0.14	0.24	1.00	-0.14	-0.02	0.23	0.20	0.22	0.07	-0.17	-0.20	-0.17
PI	0.45	-0.66	0.91	-0.14	1.00	-0.62	0.44	0.35	0.32	0.25	-0.23	-0.31	-0.02
ρ	0.76	0.82	-0.62	-0.02	-0.62	1.00	-0.43	0.15	-0.13	-0.21	0.05	0.12	0.00
w	0.40	-0.37	0.52	0.23	0.44	-0.43	1.00	0.46	0.48	0.13	-0.41	-0.46	-0.22
e	0.12	-0.19	0.38	0.20	0.35	-0.15	0.46	1.00	0.99	0.11	-0.93	-0.98	-0.22
n	0.11	-0.17	0.36	0.22	0.32	-0.13	0.48	0.99	1.00	0.06	-0.95	-1.00	-0.23
S	0.05	-0.16	0.27	0.07	0.25	-0.21	0.13	0.11	0.06	1.00	0.22	-0.04	0.02
γ	-0.07	0.09	-0.25	-0.17	-0.23	0.05	-0.41	-0.93	-0.95	0.22	1.00	0.96	0.23
γ_d	-0.09	0.15	-0.34	-0.20	-0.31	0.12	-0.46	-0.98	-1.00	-0.04	0.96	1.00	0.22
s_u	-0.11	-0.02	-0.07	-0.17	-0.02	0.00	-0.22	-0.22	-0.23	0.02	0.23	0.22	1.00

The multicollinearity between void ratio, porosity, unit weight, and dry unit weight (all $|r|$ values over 0.90) was expected because all variables describe soil density. Each variable was included in the trial linear regression and the results did not change regardless of which was kept. Therefore, dry unit was kept because it represents the soil density independent of the water content. Plasticity index was removed because the r value between plasticity index and liquid limit was 0.91. Plasticity index is the difference between the liquid limit and plastic limit, so this information was inherently redundant. Finally, percent fines and median grain size were highly correlated with an $|r|$ of 0.89. Both percent fines and median grain size have been shown as variables that directly control critical shear stress (e.g., Briaud et al., 2019). Shields (1936) established that grain size controls critical shear stress in gravel and clean sands. Many others have included median grain size to similarly describe cohesive soil erosion, however results were more variable (e.g., Briaud et al., 2011). Other researchers have noted that the erodibility of cohesive soil is controlled by the amount of cohesive material, or the percent fines over the grain size (e.g., Grabowski et al., 2011; Raudkivi, 1990). Percent fines is determined more routinely than median grain size in cohesive soils because median grain size also requires a hydrometer analysis. Therefore, percent fines was kept and median grain size was dropped to avoid multicollinearity. In summary, five variables were

removed considering multicollinearity: void ratio, porosity, unit weight, plasticity index, and median grain size.

The final step in variable selection was to select the optimum number of independent variables that would best describe the dependent variable (critical shear stress). Liquid limit was included as is and as a quadratic function adding an extra variable. The quadratic function was added because the critical shear stress increased with increasing liquid limit up to a liquid limit value of around 50 and beyond this point the critical shear stress decreased. A quadratic function modeled this behavior. The optimum number was identified with backward elimination from the nine variables. The predictive performance of a variable was evaluated based on the t-statistic and removed if not satisfactory. This process continued until all remaining variables were significant. A significance level of $\alpha = 0.10$ was chosen because 0.05 to 0.10 is commonly used (Mendenhall & Sincich, 2012) and the backward elimination result was also verified by an additional variable screening. Therefore, the more conservative significance level of 0.05 was not used so as to not over constrain the model.

Percent fines, liquid limit as a quadratic function (i.e., LL^2 and LL), and electrical resistivity were identified as significant independent variables for predicting critical shear stress based on the backward elimination process. Therefore, plastic limit, water content, saturation, dry density, and undrained shear strength were eliminated from the model. An additional variable selection algorithm via *F* scores (Equation 2.5) was used to independently validate the backward elimination variables (Pedregosa et al., 2011). The F scores shown in Table 4.3 show that percent fines, liquid limit, liquid limit as a quadratic function, and electrical resistivity were higher than the remaining five variables. This indicated they were the most influential variables. Furthermore, this result agreed with the backward elimination method.

Table 4.3: *F* Scores of the independent variables for predicting critical shear stress

Variable	$Log(f)$	LL^2	LL	PL	$Log(\rho)$	w	S	D_d	S_u
***F* score**	59.7	18.8	31.1	0.5	70.9	6.1	1.5	0.001	0.7

4.1 Model to Predict Critical Shear Stress in Cohesive Soils

The multiple linear regression analysis was run on the independent variables selected from the variable screening process. The four independent variables were: percent fines, liquid limit, liquid limit squared, and electrical resistivity. Although the original sample set included 70 samples, the critical shear stress of five samples were above 1.2 lb/ft^2. This would generally be considered rock in terms of an erosion index and the model with or without these samples could not predict this high. The same independent variables were identified via backwards elimination and their *F* scores based on the dataset with 65 observations, therefore the five observations above 1.2 lb/ft2 were removed. The result of the linear regression was:

$$\tau_c = f^{0.74}\rho^{-0.48}10^{-6.20LL^2+7.24LL-3.37} \qquad \textbf{Equation 4.1}$$

Where all variables have previously been defined and the resulting critical shear stress, τ_c, is in lb/ft^2. Note that percent fines, *f*, is taken as the percentage but *LL* is in the decimal format (typical geotechnical convention presents *LL* in percent).

The results of the measured critical shear stress versus the shear stress calculated from Equation 4.1 are shown in Figure 4.2. Over half (i.e., 36) of the 65 observations underpredicted the critical shear stress. The coefficient of determination, R^2, of the model was 0.65; this fit was considered moderate to substantial (Henseler, Ringle, & Sinkovics, 2009).

The "leave one out method" was the last step to validate model coefficients. Cross validation determines the model coefficients dependence on the observations in a data set so the model can be used for sites not used in the dataset. The leave one out method builds the model with all variables except one. In this case, 64 observations were used to build the model and the remaining observation was used for validation. This process was repeated 65 times, or the number of observations in the dataset, yielding 65 sets of intercept and coefficients along with their maximum, minimum, and mean values. Table 4.4 shows the results of the leave one out method. The mean values of the model intercept and all four coefficients were within 1% of the coefficients from the regression analysis shown in Equation 4.1. This process supported the model shown in Equation 4.1 as the final model to predict critical shear stress of cohesive soils.

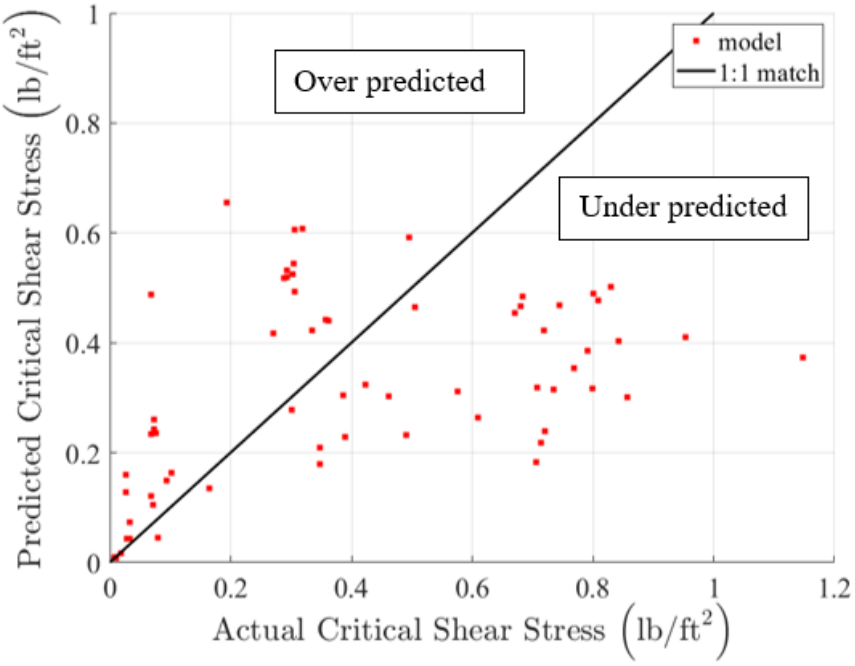

Figure 4.2: Actual (measured) versus predicted critical shear stress

Table 4.4: Model cross validation results

	Intercept	Variable Coefficients			
		$Log(f)$	LL^2	LL	$Log(\rho)$
Min.	-3.41	0.62	-8.89	5.92	-0.58
Max.	-3.32	0.84	-5.08	9.59	-0.38
Mean	-3.37	0.74	-6.23	7.27	-0.48
Selected	-3.37	0.74	-6.20	7.24	-0.48
Difference from mean	-0.00	0.00	-0.03	0.03	0.00

4.2 Highway Applications

As shown in Figure 4.2, the final model over predicted 29 of the 65 data points. In other words, the soil eroded relatively easily but was calculated to be more erosion resistant. Four of these points were approximately on the 1:1 line, indicating a negligible over prediction. However, because 25 over predicting data points remained, a reducing design factor, α_d, was added to the final model such that:

$$\tau_{c,d} = \alpha_d \left(f^{0.74} \rho^{-0.48} 10^{-6.20LL^2 + 7.24LL - 3.37} \right)$$ **Equation 4.2**

Where:

$\tau_{c,d}$ is the design critical shear stress (lb/ft2), and

α_d is reduction factor based on an acceptable level of risk to minimize the probability of over predicting the critical shear stress.

Over predicting the critical shear stress falsely indicates the soil is more resistant to erosion. Thus, over predicting the critical shear stress incorrectly predicts less erodible soil, or a smaller scour hole than what may be observed in the field.

Again, note that electrical resistivity, ρ, is in Ω-m, percent fines, *f*, is entered as percentage but *LL* is in the decimal format. The typical geotechnical convention is to present *LL* as a percent without the percent sign, therefore this number should be divided by 100 and entered as a decimal. The design factor was created with a cumulative density function (CDF) of the ratio of the over predicted observations and total observations for different α_d values. For example, α_d = 1 (unfactored equation) results in a probability of over predicting critical shear stress of 0.45 because 29 of the 65 observations were over predicted. The same procedure was repeated, varying α_d. A lognormal CDF was fit to these experimental data to extrapolate a design curve. Table 4.5 shows α_d and the resulting probability of over prediction that the engineer may select to apply this model for highway applications. It is up to the design engineer to evaluate the acceptable level of risk for the specific application and then select the corresponding α_d.

Table 4.5: Design factors for highway applications and corresponding probability of over predicting critical shear stress

Design Factor, α_d	Probability of over predicting critical shear stress (%)
1	45
0.75	33
0.5	18
0.38	10
0.25	4

The α_d was developed so the design engineer can select a probability of over predicting critical shear stress that is acceptable while still achieving a prudent design (Tucker, Briaud, Hurlebaus, Everett, & Arjwech, 2015). In other words, the engineer could select the smallest design

factor, $\alpha_d = 0.25$, which would ensure the critical shear stress would be over predicted only 4% of the time; however, the final infrastructure design would likely be overly conservative. Shan et al. (2015) and Briaud et al. (2019) developed equations for predicting critical shear stress with a reduction factor such that no more than 10% of the data were over predicted. For this model 10% probability of over predicting the critical shear stress is achieved with $\alpha_d = 0.38$. Although the unfactored equation, $\alpha_d = 1$, has a probability of over prediction of 45%, it is important to consider by how much this equation is over predicted.

The impact of the predicted critical shear stress, with and without a design factor, was evaluated on local abutment scour depth calculations in cohesive soils, using the HEC-18 (Fifth Ed.) abutment scour equation (Arneson et al. 2012) for cohesive soils defines the scour depth y_s (ft) as:

$$y_s = \alpha_B \left[\left(\frac{\gamma}{\tau_c} \right)^{\frac{3}{7}} \left(\frac{n q_{2f}}{K_u} \right)^{\frac{6}{7}} \right] - y_0 \qquad \textbf{Equation 4.3}$$

Where:

α_B (unitless) = the scour amplification factor which is dependent on unit discharge of the stream,

γ (lb/ft^3) = the unit weight of flowing water,

n (unitless) = Manning's coefficient,

q_{2f} (ft^2/s) = the abutment unit discharge,

K_u = a dimensionless factor (1.486 in English units), and

y_0 = the abutment flow depth before scour.

The values of α_B, γ, n, q_{2f}, and y_0 were assumed from a design example defined in HEC-18 as 2.1, 62.4 lb/ft^3, 0.025, 10.1 ft^2/s, and 3.5 ft, respectively (Arneson et al., 2012). The design critical shear stress was calculated based on the 65 observed data points using Equation 4.2 with two of the design factors shown in Table 4.5 (α_d = 0.5 and 1.0). These critical shear stresses were used to predict the scour depth.

Figure 4.3 compares these predicted scour depths with the calculated scour depths using the measured critical shear stress from the EFA tests (i.e., the dependent variable shown in Figure 4.1 that ranged from 0.008 to 2.03 psf). The abutment scour was also calculated using the conservative approach of assuming the smallest allowable median grain size (d_{50}) for Equation 4.3 is equal to the critical shear stress.

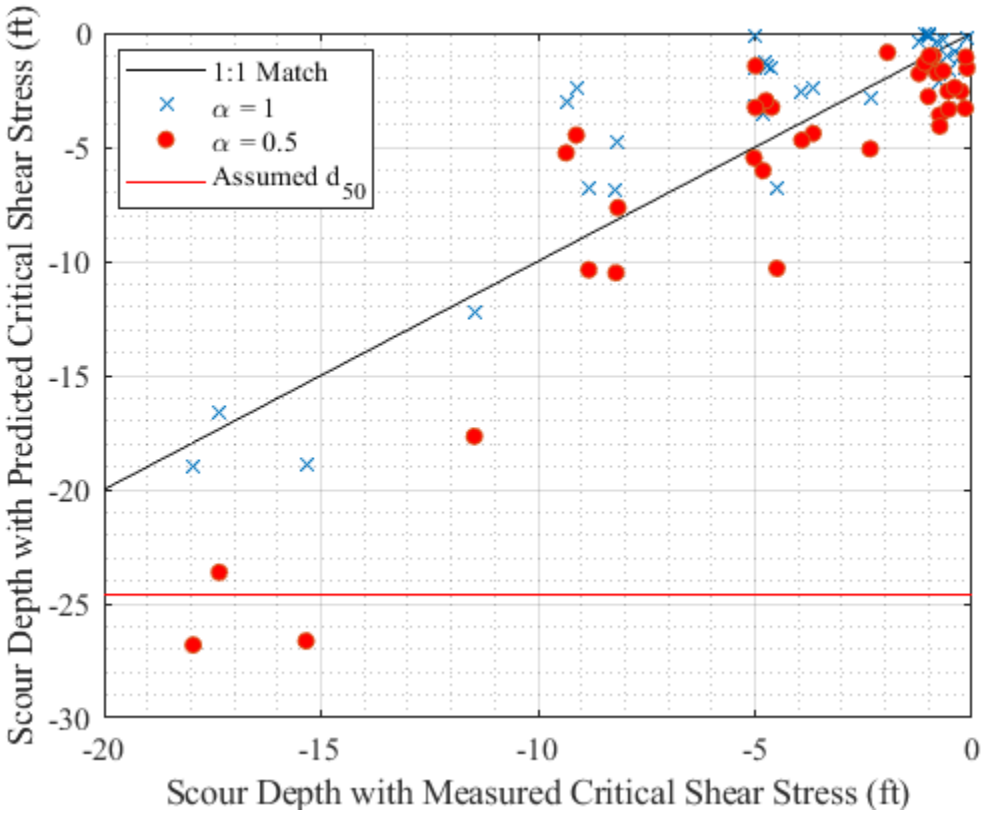

Figure 4.3: Evaluation of new model on calculated abutment scour

Figure 4.4 highlights the influence of the critical shear stress model in Equation 4.2 on the calculated abutment scour, with and without a design factor reduction, compared to the calculated abutment scour using measured critical shear stress. Overall, the unfactored equation yielded scour depths within a few feet of the scour depth (86% of the samples in this study were within two feet). An arbitrary design factor, α_d = 0.5, from Table 4.5 was chosen to highlight the influence of reducing the critical shear stress. A design factor of 0.5 will have 18% probability of over predicting the critical shear stress, but the calculated scour depths may be conservatively deeper. If a smaller probability of over predicting the critical shear stress is desired by the engineer (i.e., smaller α_d from Table 4.5), the final results will be even more conservative. Generally, these are still much less conservative than assuming a median grain size (shown with the red line). A design engineer may choose the unfactored equation to avoid extreme over prediction where the acceptable risk is higher, such as a rural structure with low volume traffic or other geotechnical structures where failure would not result in loss of life.

4.3 Validation

The final model in Equation 4.2 was validated using a site selected by the KDOT. The site is located 3.8 miles southwest of Lawrence, Kansas, along K-10. The drilling was conducted on the bank of Yankee Tank Creek and the ERT survey was conducted the same day. The subsurface electrical resistivity distribution is shown in Figure 4.4. The electrical resistivity at the sample location was 8 Ω m. The liquid limit and percent fines for the sample were 40 and 95.77, respectively. Note that all variables shown in Table 4.1 need not be measured, only the three independent variables required for Equation 4.2.

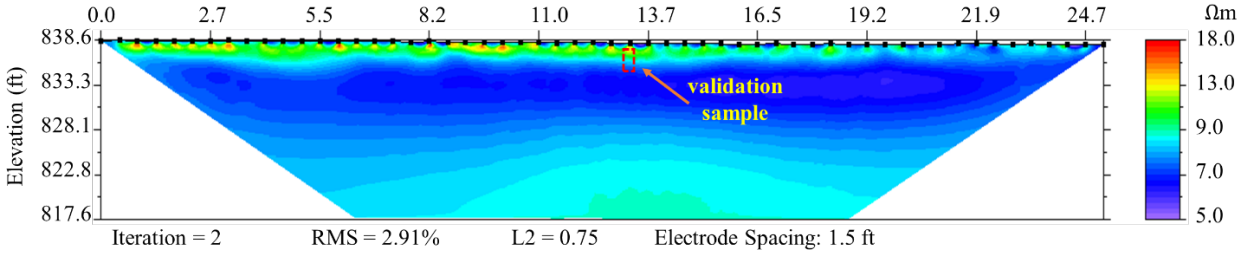

Figure 4.4: Electrical resistivity survey of K-10 over Yankee Tank Creek

The unfactored critical shear stress was 0.37 lb/ft^2 based on the measured dependent variables. As shown in Figure 4.5, the critical shear stress measured in the EFA was 0.76 lb/ft^2. Therefore, the proposed model under predicted the critical shear stress, which is conservative from design standpoint. Note that if the critical shear stress were estimated from this site assuming the critical shear stress equaled the minimum allowable median grain size in the HEC-18 for cohesionless soils, the critical shear stress would be 0.0042 psf. This is shown in Figure 4.4, resulting a scour hole of 25 ft. If the unfactored estimate of critical shear stress of 0.37 psf ($\alpha_d = 1$) is instead used, the scour hole estimate is 0.64 ft. This scour hole estimate would increase if a smaller α_d, and therefore lower acceptable risk, was assumed. Note there is no predicted scour based on the measured critical shear stress of 0.76 psf using this example. This highlights the extreme conservatism of the state of the practice, the value of the new model, and potential project savings of using the unfactored model.

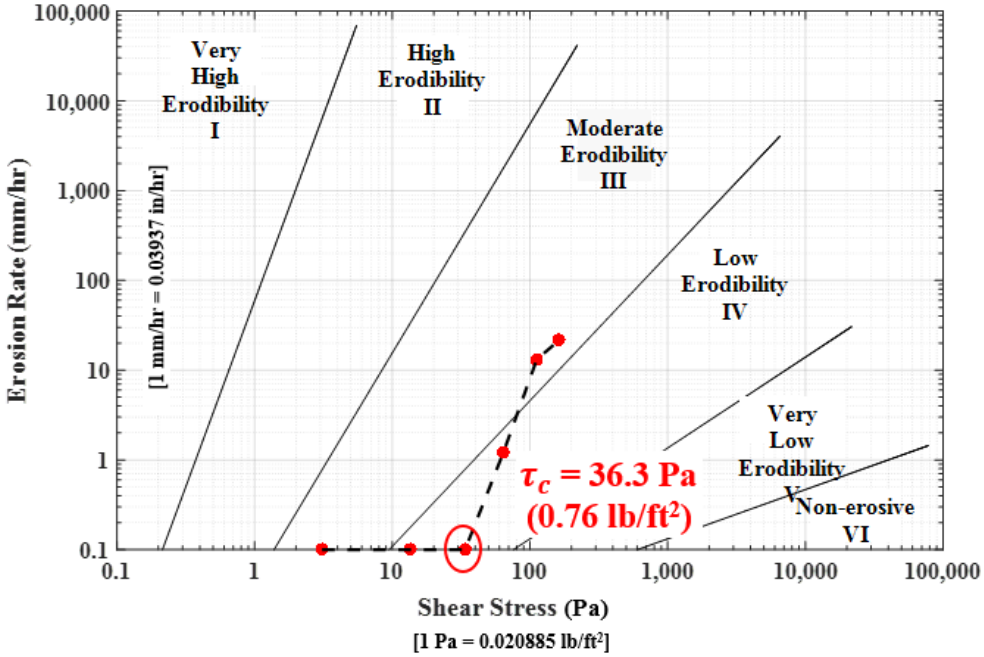

Figure 4.5: EFA results of K-10 over Yankee Tank Creek; the measured critical shear stress was 0.76 psf.

Chapter 5: Conclusions

A new model for predicting critical shear stress in cohesive soils was developed. A literature review was conducted to identify the soil properties thought to influence cohesive soil erosion. Thirteen properties were selected based on this review. Ultimately percent fines, liquid limit, and electrical resistivity were found as statistically significant independent variables for the model. This study is unique compared to other empirical models to predict critical shear stress because of the large number of samples from different sites, creating a broad spectrum of observations in cohesive soils. Furthermore, this is one of the first studies to use electrical resistivity (measured in the field or lab) as a soil property. The new model is capable of predicting critical shear stress between 0.006 and 0.66 lb/ft^2 and the model is applicable for samples with percent fines between 11 and 100, liquid limit between 26 and 80, and electrical resistivity between 6 and 328 Ω-m. Previous models on cohesive soil erosion were more limited in their predictive range and had a narrower range of soil properties. A design factor α_d was developed as a function of probability of over predicting the critical shear stress. This factor should be selected by the engineer based on the project need and the level of uncertainty they are willing to accept.

5.1 Recommendations

It is recommended that the new design equation be used for estimating the critical shear stress for abutment scour in cohesive soils in Kansas. Other highway applications where soils are partially saturated, but not inundated, may also be appropriate such as streambanks, earthen embankments, or slopes. It is recommended that engineering judgement be used to determine the acceptable risk and the appropriate design factor be selected based on this risk. Two examples with input on selecting a design factor and using them to predict critical shear stress for abutment scour are included in Appendix A, though again, the design factor should be selected by the engineer based on their accepted level of risk. Note that the most accurate method to predict the critical shear stress is to directly measure it with an erosion device, such as the EFA. This may be warranted if the acceptable risk is very low and the final design needs to be less conservative. The impacts of using an assumed minimum critical shear, the new critical shear stress equation, or the measured critical shear stress on abutment scour depth calculations were illustrated with the validation site.

5.2 Future Work

This study was limited to cohesive soils collected from river banks. Therefore, regarding bridge scour the design equation is only appropriate for abutment scour applications. There is a need to evaluate if the model is valid for samples collected from inundated river beds, where the cohesive soil properties may be different and where the critical shear stress may be lower. Note that while electrical resistivity is highly influenced by the degree of saturation, the degree of saturation of all samples in this study were above the threshold that influences resistivity. However, it is unknown how the percent fines or liquid limit vary in the river bed compared to the bank. It is recommended that a similar study be conducted in the river beds and the equation validated or modified. This bed critical shear stress should then be evaluated in pier and contraction scour equations.

Alternatively, because the equation herein was developed on the river banks, it may be appropriate in other geotechnical structures where partially saturated cohesive soils are used such as streambanks, levees, dams, and slopes. The engineer must evaluate if the soil properties at these sites are within the bounds of the model (percent fines between 11 and 100, liquid limit between 26 and 80, and electrical resistivity between 6 and 328 Ω-m). Although the model included a range of electrical resistivity, the degree of saturation was above 60% for all samples. Depending on the site characteristics, unsaturated geotechnical structures may have a lower degree of saturation, which will increase the electrical resistivity used in the model. Finally, although models to predict critical shear stress in cohesionless soils are well defined and accurate, there is very limited research on the erosion of intermediate geomaterials (IGMs). There is a need to evaluate the four sites that had very high critical shear stress, as they may not be classified as cohesive soil but cohesive IGM. Although the model is conservative for these sites, understanding their enhanced erosion resistance will help to further understand the controls on cohesive soil erosion and improve model accuracy.

References

Abu-Hassanein, Z. S., Benson, C. H., & Blotz, L. R. (1996). Electrical resistivity of compacted clays. *Journal of Geotechnical Engineering, 122*(5), 397–406.

Advanced Geosciences, Inc. (AGI). (2009). *Instruction manual for EarthImager 2D version 2.4.0 resistivity and IP inversion software*. Austin, TX: Author.

Ahmed, A., Hossain, S., & Khan, M. S. (2018). Monitoring of moisture variation in highway slope through resistivity imaging. *IFCEE 2018: Innovations in ground improvement for soils, pavements, and subgrades* (pp. 435–444). Reston, VA: American Society of Civil Engineers.

Amaryan, L. S. (1993). *Soft soil properties and testing methods*. Rotterdam, Netherlands: A. A. Balkema.

Amos, C. L., Bergamasco, A., Umgiesser, G., Cappucci, S., Cloutier, D., DeNat, L., Flindt, M., Bonardi, M., & Cristante, S. (2004). The stability of tidal flats in Venice Lagoon—the results of in-situ measurements using two benthic, annular flumes. *Journal of Marine Systems, 51*(1–4), 211–241.

Amos, C. L., Feeney, T., Sutherland, T. F., & Luternauer, J. L. (1997). The stability of fine-grained sediments from the Fraser River Delta. *Estuarine, Coastal and Shelf Science, 45*(4), 507–524.

Ariathurai, R., & Arulanandan, K. (1978). Erosion rates of cohesive soils. *Journal of the Hydraulics Division, 104*(2), 279–283.

Arneson, L. A., Zevenbergen, L. W., Lagasse, P. F., & Clopper, P. E. (2012). *Evaluating scour at bridges* (Hydraulic Engineering Circular No.8 [HEC-18], 5th ed.). Washington, DC: Federal Highway Administration.

Arulanandan, K. (1975). Fundamental aspects of erosion of cohesive soils. *Journal of the Hydraulics Division, 101*(5), 635–639.

ASTM C117-17. (2017). *Standard test method for materials finer than 75-µm (No. 200) sieve in mineral aggregates by washing*. West Conshohocken, PA: ASTM International. doi: 10.1520/C0117-17, www.astm.org

ASTM C136 / C136M-14. (2014). *Standard test method for sieve analysis of fine and coarse aggregates*. West Conshohocken, PA: ASTM International. doi: 10.1520/C0136_C0136M-14, www.astm.org

ASTM D1587 / D1587M-15. (2015). *Standard practice for thin-walled tube sampling of fine-grained soils for geotechnical purposes*. West Conshohocken, PA: ASTM International. doi: 10.1520/D1587_D1587M-15, www.astm.org

ASTM D2216-19. (2019). *Standard test methods for laboratory determination of water (moisture) content of soil and rock by mass*. West Conshohocken, PA: ASTM International. doi: 10.1520/D2216-19, www.astm.org

ASTM D2850-15. (2015). *Standard test method for unconsolidated-undrained triaxial compression test on cohesive soils*. West Conshohocken, PA: ASTM International. doi: 10.1520/D2850-15, www.astm.org

ASTM D4220 / D4220M-14. (2014). *Standard practices for preserving and transporting soil samples*. West Conshohocken, PA: ASTM International. doi: 10.1520/D4220_D4220M-14, www.astm.org

ASTM D4318-17e1. (2017). *Standard test methods for liquid limit, plastic limit, and plasticity index of soils*. West Conshohocken, PA: ASTM International. doi: 10.1520/D4318-17E01, www.astm.org

ASTM D7263-09(2018)e2. (2018). *Standard test methods for laboratory determination of density (unit weight) of soil specimens*. West Conshohocken, PA: ASTM International. doi: 10.1520/D7263-09R18E02, www.astm.org

ASTM D7928-17. (2017). *Standard test method for particle-size distribution (gradation) of fine-grained soils using the sedimentation (hydrometer) analysis*. West Conshohocken, PA: ASTM International. doi: 10.1520/D7928-17, www.astm.org

ASTM G187-18. (2018). *Standard test method for measurement of soil resistivity using the two-electrode soil box method*. West Conshohocken, PA: ASTM International. doi: 10.1520/G0187-18, www.astm.org

Bale, A. J., Stephens, J. A., & Harris, C. B. (2007). Critical erosion profiles in macro-tidal estuary sediments: Implications for the stability of intertidal mud and the slope of mud banks. *Continental Shelf Research, 27*(18), 2303–2312.

Bernhardt, M., Briaud, J.-L., Kim, D., Leclair, M., Storesund, R., Lim, S.-G., Bea, R. G., & Rogers, J. D. (2011). Mississippi River levee failures: June 2008 flood. *International Journal of Geoengineering Case Histories, 2*(3), 127–162.

Binley, A., & Kemna, A. (2005). DC resistivity and induced polarization methods. In *Hydrogeophysics* (Water Science and Technology Library, vol. 50, pp. 129–156). Dordrecht, Netherlands: Springer.

Brady, Z., Parsons, R., & Han, J. (2016). *Testing aggregate backfill for corrosion potential* (Report No. K-TRAN: KU-15-5). Topeka, KS: Kansas Department of Transportation.

Briaud, J.-L., Chen, H.-C., Chang, K.-A., Oh, S. J., Chen, S., Wang, J., Li, Y., Kwak, K., Nartjaho, P., Gudaralli, R., Wei, W., Pergu, S., Cao, Y. W., & Ting, F. (2011). *The SRICOS–EFA method, Summary report*. College Station, TX: Texas A&M University.

Briaud, J.-L., Govindasamy, A. V., & Shafii, I. (2017). Erosion charts for selected geomaterials. *Journal of Geotechnical and Geoenvironmental Engineering, 143*(10). https://doi.org/10.1061/(ASCE)GT.1943-5606.0001771

Briaud, J.-L., Shafii, I., Chen, H.-C., & Medina-Cetina, Z. (2019). *Relationship between erodibility and properties of soils* (NCHRP Research Report 915). Washington, DC: Transportation Research Board.

Campos-Aranda, D. F. (2011). Transference of hydrologic information through multiple linear regression, with best predictor variables selection. *Agrociencia, 45*(8), 863–880.

Chen, Y., Wei, Z., Irfan, M., Xu, J., & Yang, Y. (2018). Laboratory investigation of the relationship between electrical resistivity and geotechnical properties of phosphate tailings. *Measurement, 126*, 289–298.

Debnath, K., Nikora, V., Aberle, J., Westrich, B., & Muste, M. (2007). Erosion of cohesive sediments: Resuspension, bed load, and erosion patterns from field experiments. *Journal of Hydraulic Engineering, 133*(5), 508–520.

Dickhudt, P. J., Friedrichs, C. T., & Sanford, L. P. (2011). Mud matrix solids fraction and bed erodibility in the York River estuary, USA, and other muddy environments. *Continental Shelf Research, 31*(10), S3–S13.

Dunn, I. S. (1959). Tractive resistance of cohesive channels. *Journal of the Soil Mechanics and Foundations Division, 85*(3), 1–24.

Everett, M. E. (2013). Chapter 4, Electrical resistivity method. *Near-surface applied geophysics* (pp. 70–102). New York, NY: Cambridge University Press.

Federal Highway Administration (FHWA). (2020). *Advanced geotechnical methods in exploration (A-GaME)*. Retrieved August 7, 2019, from https://www.fhwa.dot.gov/innovation/everydaycounts/edc_5/geotech_methods.cfm

Friedman, S. P. (2005). Soil properties influencing apparent electrical conductivity: A review. *Computers and Electronics in Agriculture, 46*(1–3), 45–70.

Fukue, M., Minato, T., Horibe, H., & Taya, N. (1999). The micro-structures of clay given by resistivity measurements. *Engineering Geology, 54*(1–2), 43–53.

Grabowski, R. C., Droppo, I. G., & Wharton, G. (2011). Erodibility of cohesive sediment: The importance of sediment properties. *Earth-Science Reviews, 105*(3–4), 101–120.

Grissinger, E. H. (1982). Bank erosion of cohesive materials. In *Gravel-bed rivers* (pp. 273-287). New York, NY: John Wiley & Sons, Ltd.

Hanson, G. J., Cook, K. R., & Simon, A. (1999). Determining erosion resistance of cohesive materials. In *ASCE Intl. Water Resources Conference Proceedings*. Reston, VA: American Society of Civil Engineers.

Hanson, G. J., & Simon, A. (2001). Erodibility of cohesive streambeds in the loess area of the midwestern USA. *Hydrological Processes, 15*(1), 23–38.

Heinzen, R. T. (1976). *Erodibility criteria for soil* (Master's thesis). University of California, Davis, CA.

Henseler, J., Ringle, C. M., & Sinkovics, R. R. (2009). The use of partial least squares path modeling in international marketing. In *New challenges to international marketing* (pp. 277–319). Bingley, UK: Emerald Group Publishing Limited.

Houwing, E.-J. (1999). Determination of the critical erosion threshold of cohesive sediments on intertidal mudflats along the Dutch Wadden Sea Coast. *Estuarine, Coastal and Shelf Science, 49*(4), 545–555.

Jepsen, R., Roberts, J., & Lick, W. (1997). Effects of bulk density on sediment erosion rates. *Water, Air, and Soil Pollution, 99*, 21–31.

Kansas Geological Survey (KGS). (n.d.). *Surficial geology of Kansas*. Retrieved August 7, 2019, from http://maps.kgs.ku.edu/state_geology/

Karim, M. Z. (2016). *Characterizing soil erosion potential using electrical resistivity imaging* (Master's thesis). Kansas State University, Manhattan, KS. Retrieved from http://krex.k-state.edu/dspace/bitstream/handle/2097/32899/MdZahidulKarim2016.pdf?sequence=1

Karim, M. Z., & Tucker-Kulesza, S. E. (2018). Predicting soil erodibility using electrical resistivity tomography. *Journal of Geotechnical and Geoenvironmental Engineering, 144*(4). https://doi.org/10.1061/(ASCE)GT.1943-5606.0001857

Karim, M. Z., Tucker-Kulesza, S. E., & Bernhardt-Barry, M. (2019). Electrical resistivity as a binary classifier for bridge scour evaluation. *Transportation Geotechnics, 19*, 146–157. https://doi.org/10.1016/j.trgeo.2019.03.002

Kibria, G. (2014). *Evaluation of physico-mechanical properties of clayey soils using electrical resistivity imaging technique* (Doctoral dissertation). University of Texas at Arlington, Arlington, TX.

Kibria, G., & Hossain, M. S. (2012). Investigation of geotechnical parameters affecting electrical resistivity of compacted clays. *Journal of Geotechnical and Geoenvironmental Engineering, 138*(12), 1520–1529. https://doi.org/10.1061/(ASCE)GT.1943-5606.0000722

Kimiaghalam, N., Clark, S. P., & Ahmari, H. (2015). An experimental study on the effects of physical, mechanical, and electrochemical properties of natural cohesive soils on critical shear stress and erosion rate. *International Journal of Sediment Research, 31*(1), 1–15.

Knapen, A., Poesen, J., Govers, G., Gyssels, G., & Nachtergaele, J. (2007). Resistance of soils to concentrated flow erosion: A review. *Earth-Science Reviews, 80*(1–2), 75–109.

Kouchaki, B., Bernhardt-Barry, M., Wood, C., & Moody, T. (2018). A laboratory investigation of factors influencing the electrical resistivity of different soil types. *Geotechnical Testing Journal, 42*(4), 829–853.

Leeder, M. R. (1999). *Sedimentology and sedimentary basins: From turbulence to tectonics*. Oxford, UK: Blackwell Science.

Lick, W., & McNeil, J. (2001). Effects of sediment bulk properties on erosion rates. *Science of the Total Environment, 266*(1–3), 41–48.

Mahalder, B., Schwartz, J. S., Palomino, A. M., & Zirkle, J. (2018). Relationships between physical-geochemical soil properties and erodibility of streambanks among different physiographic provinces of Tennessee, USA. *Earth Surface Processes and Landforms, 43*(2), 401–416.

McCarter, W. J. (1984). The electrical resistivity characteristics of compacted clays. *Geotechnique, 34*(2), 263–267.

Mendenhall, W., & Sincich, T. (2012). *A second course in statistics: Regression analysis* (7th ed.). Boston, MA: Prentice Hall.

Mitchell, J. K., & Soga, K. (2005). *Fundamentals of soil behavior* (3rd ed.). Hoboken, NJ: John Wiley & Sons, Inc.

Moody, L. F. (1944). Friction factors for pipe flow. *Transactions of the ASME, 66*(8), 671–684.

Neuendorf, K. K. E., Mehl, J. P., Jr., & Jackson, J. A. (2011). *Glossary of geology* (5th ed., revised). Alexandria, VA: American Geological Institute.

Panagiotopoulos, I., Voulgaris, G., & Collins, M. B. (1997). The influence of clay on the threshold of movement of fine sandy beds. *Coastal Engineering, 32*(1), 19–43.

Partheniades, E. (1965). Erosion and deposition of cohesive soils. *Journal of the Hydraulics Division, 91*(1), 105–139.

Paterson, D. M. (1997). Biological mediation of sediment erodibility: Ecology and physical dynamics. In N. Burt, R. Parker, & J. Watts (Eds), *Cohesive sediments* (pp. 215–229). New York, NY: John Wiley and Sons.

Pedregosa, F., Varoquaux, G., Gramfort, A., Michel, V., Thirion, B., Grisel, O., Blondel, M., Prettenhofer, P., Weiss, R., Dubourg, V., Vanderplas, J., Passos, A., Cournapeau, D., Brucher, M., Perrot, M., & Duchesnay, E. (2011). Scikit-learn: Machine learning in Python. *Journal of Machine Learning Research, 12*(85), 2825-2830.

Raudkivi, A. J. (1990). *Loose boundary hydraulics* (3rd ed.). New York, NY: Pergamon Press.

SAS Institute, Inc. (2014). SAS™ [Computer software]. Cary, NC: SAS Institute, Inc.

Shan, H., Shen, J., Kilgore, R., & Kerenyi, K. (2015). *Scour in cohesive soils* (Report No. FHWA-HRT-15-033). McLean: VA: Federal Highway Administration.

Shields, A. (1936). *Anwendung der aenlichkeitsmechanik und der turbulenzforschung auf die geschiebebewegung* [Application of similarity principles and turbulence research to bed-load movement] (Doctoral dissertation, W. P. Ott & J. C. Van Uchelen, Trans.). Pasadena, CA: California Institute of Technology.

Smerdon, E. T., & Beasley, R. P. (1961). Critical tractive forces in cohesive soils. *Agricultural Engineering, 42*(1), 26–29.

Thoman, R. W., & Niezgoda, S. L. (2008). Determining erodibility, critical shear stress, and allowable discharge estimates for cohesive channels: Case study in the Powder River Basin of Wyoming. *Journal of Hydraulic Engineering, 134*(12), 1677–1687.

Tucker, S. E., Briaud, J.-L., Hurlebaus, S., Everett, M. E., & Arjwech, R. (2015). Electrical resistivity and induced polarization imaging for unknown bridge foundations. *Journal of Geotechnical and Geoenvironmental Engineering, 141*(5). https://doi.org/10.1061/(ASCE)GT.1943-5606.0001268

Tucker-Kulesza, S., & Karim, M. Z. (2017). *Characterizing soil erosion potential using electrical resistivity imaging* (Report No. K-TRAN: KSU-15-4). Topeka, KS: Kansas Department of Transportation.

Tucker-Kulesza, S., Snapp, M., & Koehn, W. (2016). *Electrical resistivity measurement of mechanically stabilized earth wall backfill* (Report No. K-TRAN: KSU-15-6). Topeka, KS: Kansas Department of Transportation.

Utley, B. C., & Wynn, T. M. (2008). Cohesive soil erosion: Theory and practice. *World Environmental and Water Resources Congress 2008: Ahupua'A*. Reston, VA: American Society of Civil Engineers.

Van Ledden, M., Van Kesteren, W. G. M., & Winterwerp, J. C. (2004). A conceptual framework for the erosion behavior of sand–mud mixtures. *Continental Shelf Research, 24*(1), 1–11.

Widdows, J., Brinsley, M. D., & Pope, N. D. (2009). Effect of Nereis diversicolor density on the erodability of estuarine sediment. *Marine Ecology Progress Series, 378*, 135–143.

Winterwerp, J. C., & van Kesteren, W. G. M. (2004). *Introduction to the physics of cohesive sediment dynamics in the marine environment, Volume 56*. Amsterdam, Netherlands: Elsevier Science.

Yoo, C., & Cho, E. (2019). Effect of multicollinearity on the bivariate frequency analysis of annual maximum rainfall events. *Water, 11*(5), 905.

Zeller, D. E. (1968). *The stratigraphic succession in Kansas* (Bulletin 189). Lawrence, KS: Kansas Geological Survey.

Zonge, K., Wynn, J., & Urquhart, S. (2005). Chapter 9: Resistivity, induced polarization, and complex resistivity. In *Near-surface geophysics* (pp. 265–300). Tulsa, OK: Society of Exploration Geophysics.

Appendix A: Design Examples

Note that the following examples are only shown to emphasize the effects of the "Design Factor" on abutment scour depths. For a complete abutment scour design, see the current version of HEC-18 "Evaluating Scour at Bridges".

Example 1

Due to increased AADT, a portion of I-70 requires additional east and west bound lanes. An old two-span bridge in this section with an unknown foundation must be replaced to facilitate the additional lanes. A geotechnical investigation from the stream bank classified soils as fat clay with 97% fines, liquid limit 57 and plasticity index 34. An electrical resistivity survey showed that soils from the proposed abutment location had an electrical resistivity of 7 Ωm. Note that the spill through abutment is set back from the channel such that L/B_f = 0.5 (where, L is the length of embankment into the floodplain and B_f is the distance between stream bank and edge of highway along the floodplain), upstream floodplain unit discharge = 17.2 ft^2/s, abutment unit discharge =37.8 ft^2/s, abutment flow depth before scour = 8 ft. Assume Manning's coefficient = 0.027. **Select a design factor, determine the design critical shear stress initiating scour, and calculate the abutment scour depth for clear water scour.**

Given:

Percent fines, f = 97

Liquid limit, LL = 57

Electrical resistivity, ρ = 7 Ωm

abutment unit discharge, q_{2f} = 37.8 ft^2/s

upstream floodplain unit discharge, q_f = 17.2 ft^2/s

Ratio of discharge, q_{2f}/q_f = 37.8/17.2 =2.2

abutment flow depth before scour y_0= 8 ft

Dimensionless factor, K_u = 1.486

Unit weight of water, γ = 62.4 lb/ft^3

Manning's coefficient, n = 0.027

Determine:

The critical shear stress design factor, α_d

Design critical shear stress, $\tau_{c,d}$

Abutment scour depth, y_s

Solution:

Design Critical Shear Stress:

From Equation 4.1, the critical shear stress is

$$\tau_c = \left(f^{0.74}\rho^{-0.48}10^{-6.20LL^2+7.24LL-3.37}\right)$$

$$= 97^{0.74} * 7^{-0.48} * 10^{-6.2(0.57)^2+7.24*0.57-3.37}$$

= 0.64 lb/ft^2

Design factor:

The scour design on a major interstate highway with high traffic volume is a high value project, which corresponds to a scour design flood frequency of Q100. Assume a design factor α_d = 0.38 because this associated with a probability of 10% of over predicting the critical shear stress, which is the acceptable risk for critical shear stress identified by the FHWA (Shan et al., 2015).

From Equation 4.2 and the selected design factor, the design critical shear stress,

$$\tau_{c,d} = \alpha_d * \ 97^{0.74} * 7^{-0.48} * 10^{-6.2(0.57)^2+7.24*0.57-3.37} = 0.38 * 0.64$$

= **0.24 lb/ft^2**

Calculate the abutment scour depth per the HEC-18 clear water abutment scour equation:

Flow depth, $y_c = \left(\frac{\gamma}{\tau_c}\right)^{\frac{3}{7}}\left(\frac{nq_{2f}}{K_u}\right)^{\frac{6}{7}} = \left(\frac{62.4}{0.24}\right)^{\left(\frac{3}{7}\right)} * \left(\frac{0.027*37.8}{1.486}\right)^{\frac{6}{7}} = 7.85$ ft

For q_{2f}/q_f = 2.2 the scour amplification factor α_B = 1.9 (Figure A.1)

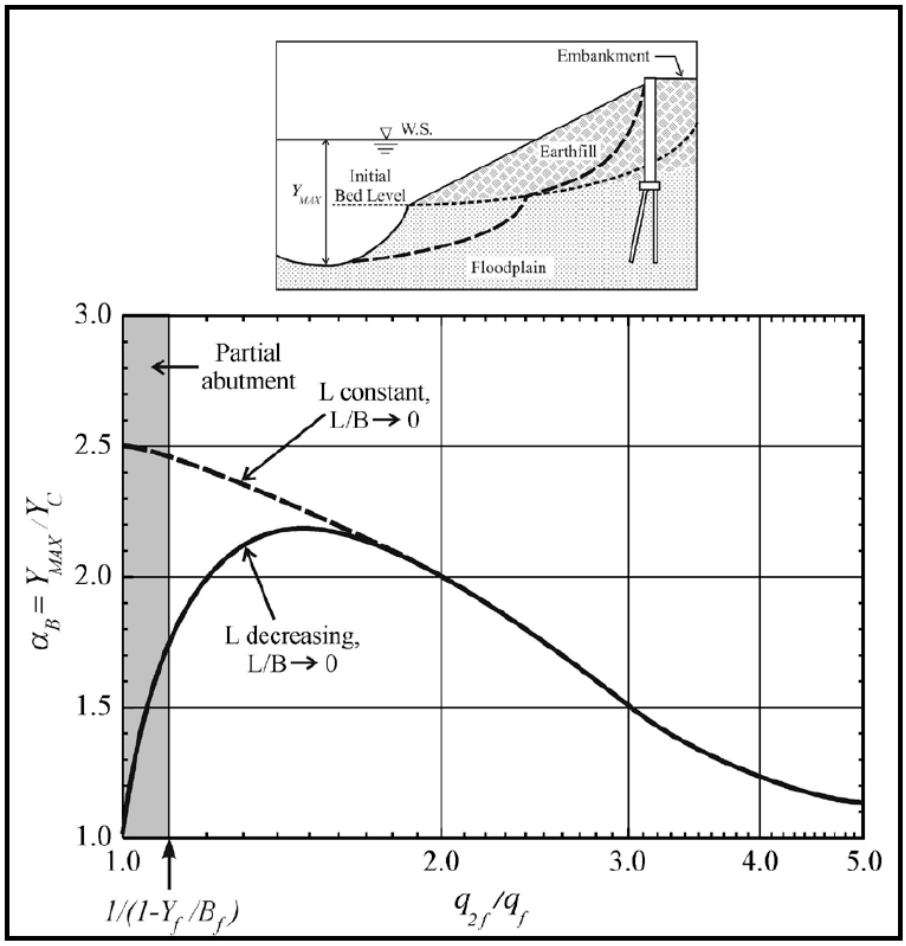

Figure A.1: Scour amplification factor for spill-through abutments and clear water conditions

Source: Arneson et al. (2012)

Maximum flow depth resulting from abutment scour, $y_{mx} = \alpha_B y_c = 1.9 * 7.85 = 14.5\ ft$

Abutment scour depth, $y_s = y_{mx} - y_0 = 14.5 - 8 = 6.9$ ft

Example 2

A new single span bridge will be constructed for a rural highway in southeast Kansas. A geotechnical investigation from the river bank, parallel to the old bridge, classified soils as lean clay with 91% fines, liquid limit 38 and plasticity index 21. An electrical resistivity survey showed that soils from the proposed abutment location had an electrical resistivity of 18 Ωm. The spill through abutment is set back from the channel such that L/B_f = 0.6 (where, L is the length of the embankment into the floodplain and B_f is the distance between the stream bank and highway edge along the floodplain). The upstream floodplain unit discharge = 6.2 ft^2/s, abutment unit discharge = 11.2 ft^2/s, and the abutment flow depth before scour = 3 ft. **Determine the design critical shear stress and calculate the abutment scour depth for clear water scour.** Assume Manning's coefficient, n = 0.025.

Given:

Percent fines, f = 91

Liquid limit, LL = 38

Electrical resistivity, ρ = 18 Ωm

abutment unit discharge, q_{2f} = 11.2 ft^2/s

upstream floodplain unit discharge, q_f = 6.2 ft^2/s

Ratio of discharge, q_{2f}/q_f = 11.2/6.2 = 1.81

abutment flow depth before scour y_0= 3 ft

Dimensionless factor, K_u = 1.486

Unit weight of water, γ = 62.4 lb/ft^3

Manning's coefficient, n = 0.025

Determine:

Design critical shear stress, $\tau_{c,d}$

Abutment scour depth, y_s

Solution:

Design Critical Shear Stress:

From Equation 4.1, the critical shear stress is

$\tau_c = \left(f^{0.74}\rho^{-0.48}10^{-6.20LL^2+7.24LL-3.37}\right)$

$=91^{0.74} * 18^{-0.48}10^{-6.2*0.38^2+7.24*0.38-3.37}$

= 0.22 lb/ft^2

Design factor:

A less conservative and economic scour design on a rural highway with low traffic volume is warranted here. A design factor α_d = 0.75 (33% probability of over predicting critical shear stress) is chosen from Table 4.5.

From Equation 4.2, the design critical shear stress is

$\tau_{c,d} = \alpha_d * 91^{0.74} * 18^{-0.48}10^{-6.2*0.38^2+7.24*0.38-3.37}$

$= 0.75 * 91^{0.74} * 18^{-0.48}10^{-6.2*0.38^2+7.24*0.38-3.37}$= 0.75 x 0.22 = **0.17 lb/ft^2**

Calculate the abutment scour depth per the HEC-18 clear water abutment scour equation:

Flow depth, $y_c = \left(\frac{\gamma}{\tau_c}\right)^{\frac{3}{7}}\left(\frac{nq_{2f}}{K_u}\right)^{\frac{6}{7}} = \left(\frac{62.4}{0.17}\right)^{\left(\frac{3}{7}\right)} * \left(\frac{0.025*11.2}{1.486}\right)^{\frac{6}{7}} = 3.01$ ft

For q_{2f}/q_f = 1.81, the scour amplification factor α_B = 2.1 (Figure A.1)

Maximum flow depth resulting from abutment scour, $y_{mx} = \alpha_B y_c = 2.1 * 3.01 = 6.32\ ft$

Abutment scour depth, $y_s = y_{mx} - y_0 = 6.32 - 3.0 =$ **3.32 ft**

Appendix B: Inverted Resistivity Sections of New Bridge Sites

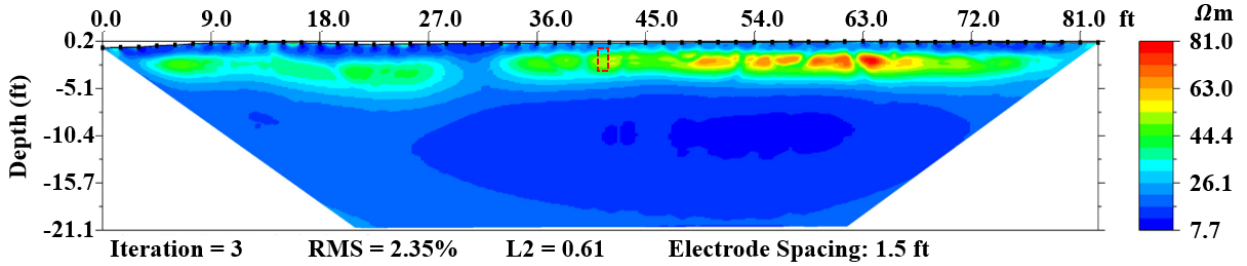

Figure B.1: Inverted resistivity section for US-24 over Asher Creek

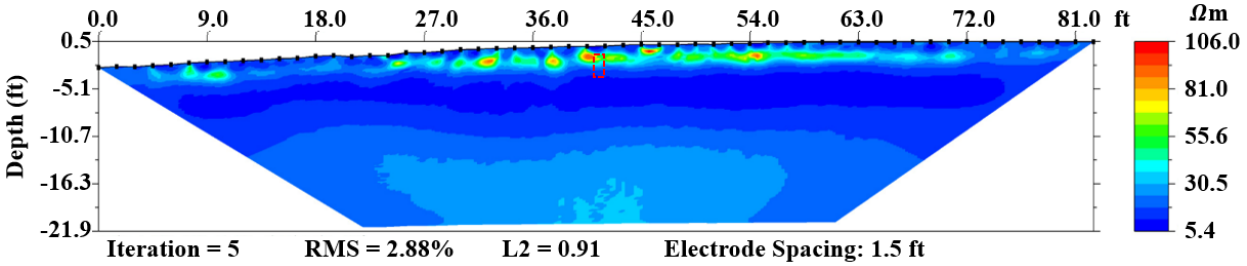

Figure B.2: Inverted resistivity section for K-68 over Marais de Cygnes

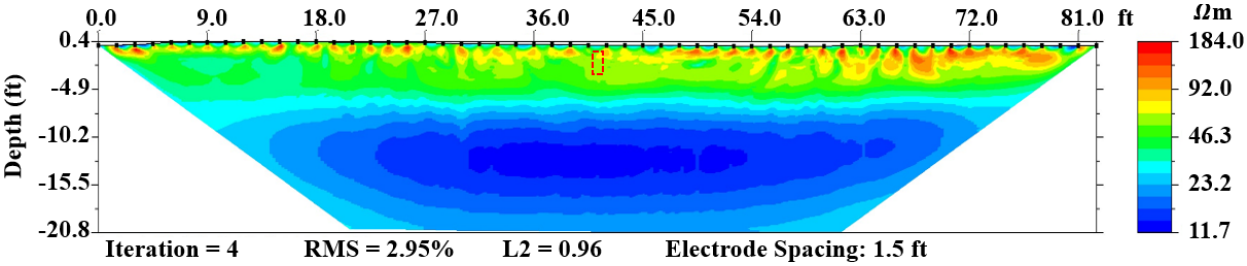

Figure B.3: Inverted resistivity section for US-24 and Menoken Road

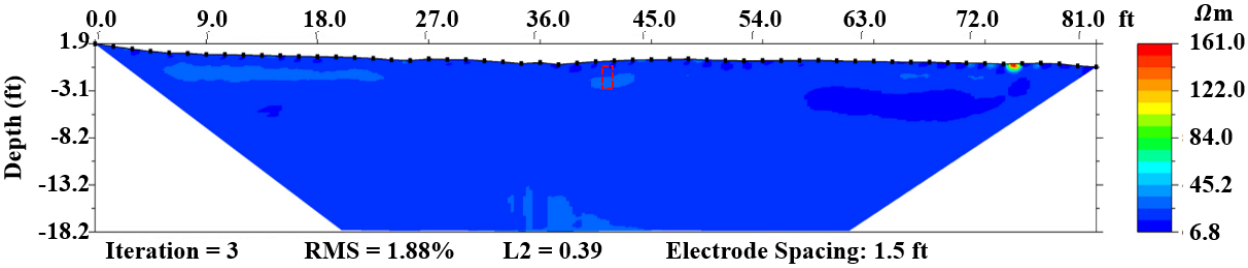

Figure B.4: Inverted resistivity section for US-160 over Neosho River overflow

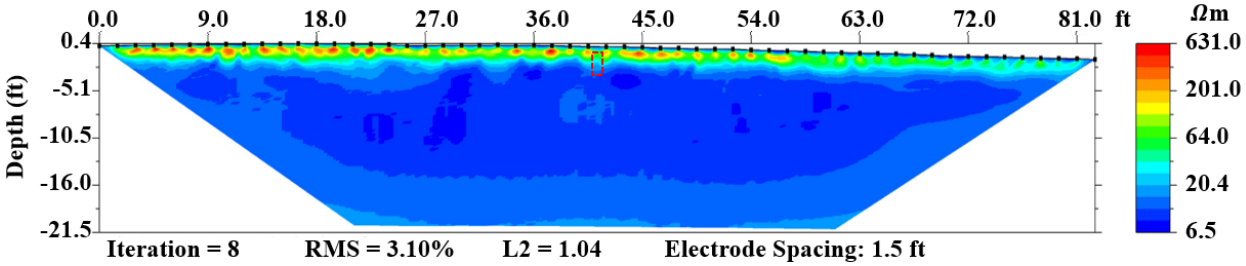

Figure B.5: Inverted resistivity section for K-148 over Parsons Creek

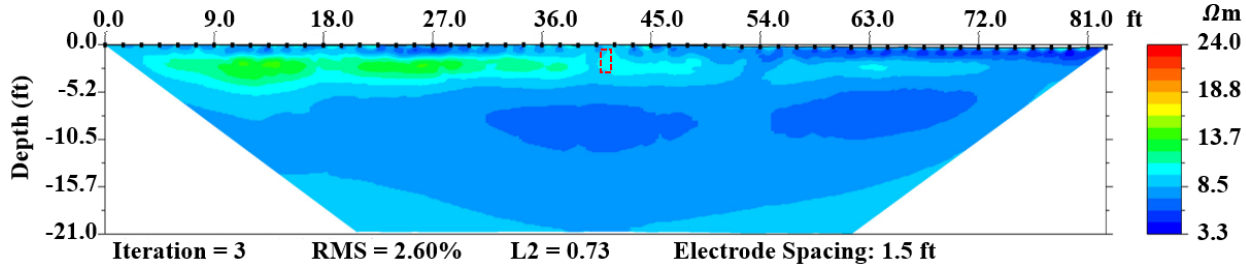

Figure B.6: Inverted resistivity section for K-15 over Smoky Hill River

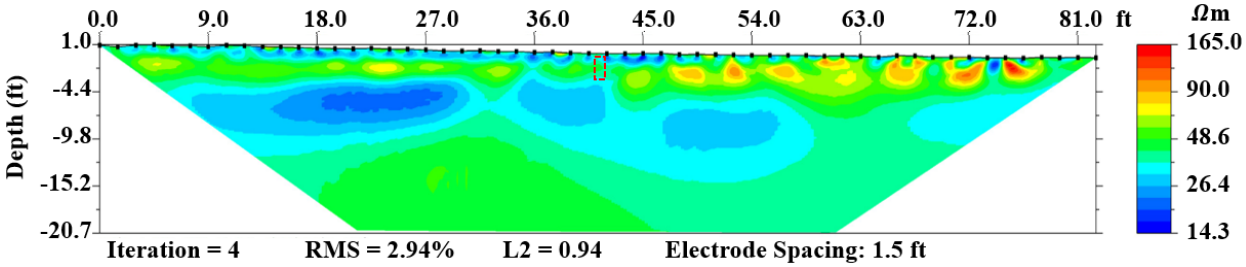

Figure B.7: Inverted resistivity section for US-24 near UP railroad

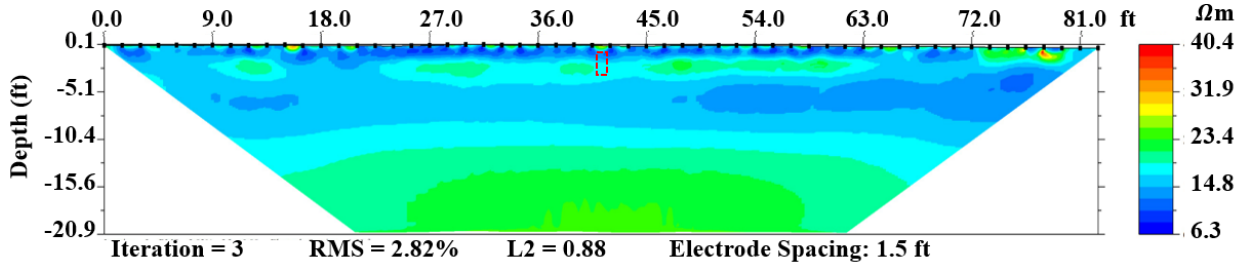

Figure B.8: Inverted resistivity section for US-166 over Neosho River drainage

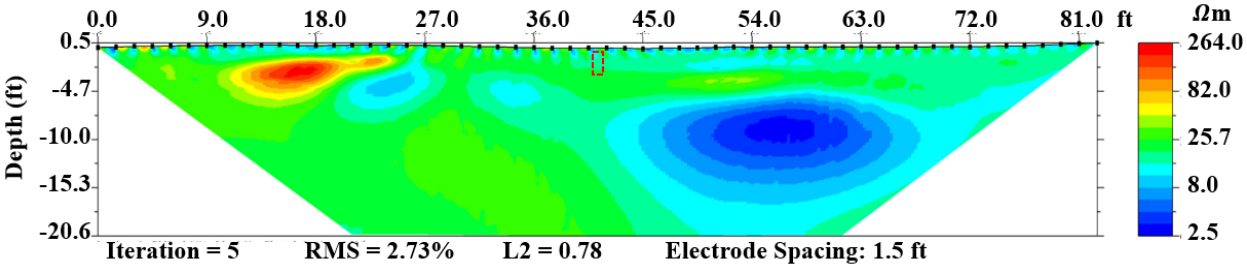

Figure B.9: Inverted resistivity section for K-58 over Neosho River drainage

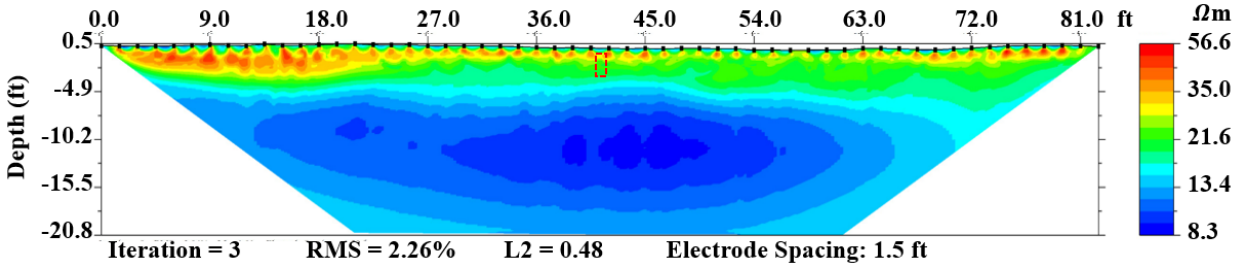

Figure B.10: Inverted resistivity section for K-28 over Wolf Creek

Appendix C: Measured Soil Properties

Site No. / Highway	Critical Shear Stress	Electrical Resistivity	Water Content	Percent Finer #200	Median Grain Size	LL	PL	PI	Void Ratio	Porosity	Degree of Saturation	Wet density	Dry density	Undrained Shear Strength
	psf	Ohm-m	%	%	inch	%	%	%			%	pcf	pcf	psf
1. K-4A	0.3050	9.52	39.65	96.50	0.00039	55	18	37	0.8531	0.4604	88.99	117.04	91.47	3000
2. K-4A	0.0737	18.19	30.23	92.37	0.00055	40	17	23	0.8531	0.4604	88.99	117.04	91.47	2500
3. K-4A	0.0262	19.38	23.23	90.41	0.00063	31	19	12	0.8531	0.4604	88.99	117.04	91.47	2300
4. K-4A	0.0682	18.81	24.39	91.28	0.00067	30	20	10	0.8531	0.4604	88.99	117.04	91.47	4000
5. K-4A	0.1644	17.94	27.25	91.71	0.00067	31	17	14	0.8531	0.4604	88.99	117.04	91.47	2500
6. US-400	0.7348	11.13	21.32	89.22	0.00047	41	14	27	0.6158	0.3811	94.89	125.85	103.27	3000
7. US-400	0.6798	12.51	20.96	96.75	0.00027	53	16	37	0.6158	0.3811	94.89	125.85	103.27	3000
8. US-400	0.3025	9.68	23.23	96.37	0.00026	53	15	38	0.6158	0.3811	94.89	125.85	103.27	1500
9. US-400	0.5758	12.62	24.50	95.30	0.00047	41	14	27	0.6158	0.3811	94.89	125.85	103.27	2250
10. K-126	0.0288	131.93	21.32	73.38	0.00075	31	22	9	0.7457	0.4272	89.72	119.52	95.59	5000
11. K-126	0.0183	327.67	18.18	48.81	0.00323	28	18	10	0.7457	0.4272	89.72	119.52	95.59	1500
12. K-126	0.0107	257.31	24.93	17.46	0.07087	26	18	8	0.7457	0.4272	89.72	119.52	95.59	1250
13. K-126	0.0085	189.37	16.76	17.62	0.06457	27	20	7	0.7457	0.4272	89.72	119.52	95.59	500
14. K-126	0.0079	136.69	23.54	11.37	0.07559	26	19	7	0.7457	0.4272	89.72	119.52	95.59	5000
15. US-75	0.2708	16.21	36.17	98.67	0.00058	53	23	30	0.7586	0.4314	90.08	120.64	96.38	1250
16. US-75	0.5048	14.09	28.41	98.76	0.00043	58	23	35	0.7586	0.4314	90.08	120.64	96.38	750
17. US-75	0.3579	10.64	25.41	98.28	0.00059	47	24	23	0.7586	0.4314	90.08	120.64	96.38	1000
18. US-75	0.6834	10.20	29.84	96.48	0.00037	50	26	24	0.7586	0.4314	90.08	120.64	96.38	750
19. US-73	0.0689	5.98	27.24	95.21	0.00039	43	16	27	0.9170	0.4784	89.52	113.78	87.05	2750
20. US-73	0.4960	6.73	28.21	96.74	0.00024	50	17	33	0.9170	0.4784	89.52	113.78	87.05	2750
21. US-73	0.1938	6.76	26.63	98.45	0.00026	56	17	39	0.9170	0.4784	89.52	113.78	87.05	2750
22. US-73	0.3195	6.76	27.63	97.61	0.00017	51	17	34	0.9170	0.4784	89.52	113.78	87.05	1250
23. US-73	0.3068	7.04	28.49	95.91	0.00040	45	16	29	0.9170	0.4784	89.52	113.78	87.05	1250
24. US-24	0.0764	35.58	33.36	95.97	0.00089	46	21	25	0.7421	0.4260	87.16	119.06	95.94	1417
25. US-24	0.0736	17.52	30.89	95.95	0.00089	41	24	17	0.7421	0.4260	87.16	119.06	95.94	2500
26. US-24	0.0689	13.03	29.31	97.38	0.00091	36	19	17	0.7421	0.4260	87.16	119.06	95.94	3250

Site No. / Highway	Critical Shear Stress	Electrical Resistivity	Water Content	Percent Finer #200	Median Grain Size	LL	PL	PI	Void Ratio	Porosity	Degree of Saturation	Wet density	Dry density	Undrained Shear Strength
	psf	Ohm-m	%	%	inch	%	%	%			%	pcf	pcf	psf
27. K-58	0.4617	8.73	32.50	99.54	0.00005	80	28	52	1.1799	0.5413	98.41	111.00	77.75	2250
28. K-58	0.6704	8.68	32.44	99.55	0.00006	72	22	50	1.1799	0.5413	98.41	111.00	77.75	2250
29. K-58	0.3356	8.68	25.99	99.72	0.00040	43	16	27	1.1799	0.5413	98.41	111.00	77.75	2250
30. K-58	1.1479	12.31	27.66	99.79	0.00028	44	14	30	1.1799	0.5413	98.41	111.00	77.75	1100
31. K-58	0.6099	18.54	29.69	97.58	0.00057	41	25	16	1.1799	0.5413	98.41	111.00	77.75	1400
32. US-69	0.0328	39.77	16.30	60.53	0.00122	32	29	3	0.4904	0.3290	95.94	133.89	114.18	3500
33. US-69	0.7691	14.59	30.81	98.47	0.00032	45	10	35	0.4904	0.3290	95.94	133.89	114.18	2250
34. US-69	0.2932	7.84	30.10	99.43	0.00020	48	20	28	0.4904	0.3290	95.94	133.89	114.18	2250
35. US-69	0.9534	7.49	29.41	99.19	0.00025	41	24	17	0.4904	0.3290	95.94	133.89	114.18	2750
36. US-69	0.8004	9.28	26.40	99.37	0.00041	48	17	31	0.4904	0.3290	95.94	133.89	114.18	2750
37. US-166B	0.8088	12.65	28.10	98.71	0.00022	54	19	35	0.8738	0.4663	92.78	117.46	90.45	2750
38. US-166B	0.8578	12.03	27.75	94.46	0.00043	40	23	17	0.8738	0.4663	92.78	117.46	90.45	2000
39. US-166B	0.3862	10.37	29.15	93.91	0.00055	39	16	23	0.8738	0.4663	92.78	117.46	90.45	1000
40. US-166B	0.8299	9.65	29.00	97.94	0.00027	50	20	30	0.8738	0.4663	92.78	117.46	90.45	2000
41. US-166B	0.8421	9.36	29.40	98.30	0.00035	43	21	22	0.8738	0.4663	92.78	117.46	90.45	2750
42. US-54	0.7072	12.77	22.91	98.94	0.00029	41	20	21	0.5402	0.3507	78.03	125.43	108.34	3500
43. US-54	0.4229	13.50	23.89	98.61	0.00032	42	22	20	0.5402	0.3507	78.03	125.43	108.34	3250
44. US-54	0.7204	14.16	24.50	97.52	0.00026	37	19	18	0.5402	0.3507	78.03	125.43	108.34	2500
45. US-54	0.7137	14.70	25.52	95.94	0.00043	36	20	16	0.5402	0.3507	78.03	125.43	108.34	1750
46. US-54	0.3470	14.94	25.74	91.88	0.00047	36	16	20	0.5402	0.3507	78.03	125.43	108.34	1750
47. US-160	0.2931	9.04	28.34	98.35	0.00013	50	26	24	0.8911	0.4712	90.58	116.27	89.63	986
48. US-160	0.7187	9.26	29.69	98.13	0.00020	44	22	22	0.8911	0.4712	90.58	116.27	89.63	2250
49. US-160	0.2886	9.07	26.28	97.88	0.00024	50	24	26	0.8911	0.4712	90.58	116.27	89.63	2250
50. US-160	0.3620	9.11	24.54	97.39	0.00024	45	20	25	0.8911	0.4712	90.58	116.27	89.63	2250
51. US-160	0.7441	9.36	28.50	97.79	0.00020	47	22	25	0.8911	0.4712	90.58	116.27	89.63	2000
52. US-24 near UP railroad	0.0325	41.69	22.41	53.11	0.00244	27	16	11	0.8152	0.4491	78.33	114.04	92.10	902
53. K-15 over Smoky hill	0.4915	10.39	28.68	99.16	0.00114	34	23	11	0.6820	0.4055	96.93	123.88	99.49	1485

Site No. / Highway	Critical Shear Stress	Electrical Resistivity	Water Content	Percent Finer #200	Median Grain Size	LL	PL	PI	Void Ratio	Porosity	Degree of Saturation	Wet density	Dry density	Undrained Shear Strength
	psf	Ohm-m	%	%	inch	%	%	%			%	pcf	pcf	psf
54. US-24 & Menoken Rd	0.0722	61.00	32.84	98.28	0.00130	35	27	8	0.9581	0.4893	95.64	116.13	86.91	291
55. K-10 over Yankee Tank Ck	1.6119	11.42	26.28	98.65	0.00017	52	25	27	0.7859	0.4400	94.14	120.77	94.91	1721
56 K-148 over Parsons Ck	0.3898	22.18	21.52	96.79	0.00055	40	26	14	0.9542	0.4883	72.00	109.03	87.08	737
57. US-24 over Asher Ck	0.7068	36.46	27.09	98.74	0.00075	40	22	18	0.7983	0.4439	67.50	111.51	92.80	1087
58. K-68 over Marias de Cygnes	2.0279	7.66	25.40	96.13	0.00039	46	26	20	0.7414	0.4257	99.15	122.18	95.83	2443
59. US-166 over Neosho River Drainage	1.5019	17.56	24.71	97.91	0.00022	50	23	27	0.7779	0.4375	91.82	120.62	95.63	1424
60. US-160 over Neosho River Overflow	1.4182	23.40	26.16	95.90	0.00039	37	22	15	0.6545	0.3956	94.26	124.13	100.86	790
61. K-58 over Neosho River Dr	0.0273	19.53	27.08	90.32	0.00067	34	22	12	0.6396	0.3901	94.02	124.70	101.80	1276
62. K-28 over Wolf Ck	0.1024	22.76	18.91	93.64	0.00106	35	22	13	0.5417	0.3514	90.73	129.84	109.94	1991
63. US-166A	1.4416	11.16	25.14	97.73	0.00015	46	26	20	0.6640	0.3990	96.58	124.34	100.28	3750
64. US-166A	0.7904	12.40	25.87	99.33	0.00017	45	21	24	0.6640	0.3990	96.58	124.34	100.28	2000
65. US-166A	0.8000	12.96	26.93	99.59	0.00032	41	21	20	0.6640	0.3990	96.58	124.34	100.28	1000
66. US-166A	0.3016	13.03	27.78	96.78	0.00039	39	19	20	0.6640	0.3990	96.58	124.34	100.28	1750
67. US-166A	0.3471	13.04	29.41	89.56	0.00059	33	18	15	0.6640	0.3990	96.58	124.34	100.28	1500
68. Ohio	0.0792	31.27	10.84	52.07	0.00224	26	15	11	0.2819	0.2199	98.54	145.01	131.48	2262
69. Nebraska	0.0942	16.72	32.90	91.14	0.00083	32	24	8	1.0180	0.5045	86.39	109.90	82.66	744
70. Colorado	0.3057	7.20	38.14	93.55	0.00028	62	34	28	0.9987	0.4997	99.76	115.45	84.33	741

AD ASTRA PER ASPERA

Kansas

Department of Transportation